

# Depth Profiles and the Geometric Exploration of Random Objects Through Optimal Transport

Paromita Dubey<sup>\*1</sup>, Yaqing Chen<sup>\*2</sup>, and Hans-Georg Müller<sup>†2</sup>

<sup>1</sup>Department of Data Sciences and Operations, Marshall School of Business, University of Southern California

<sup>2</sup>Department of Statistics, University of California, Davis

## Abstract

We propose new tools for the geometric exploration of data objects taking values in a general separable metric space  $(\Omega, d)$ . Given a probability measure on  $\Omega$ , we introduce *depth profiles*, where the depth profile of an element  $\omega \in \Omega$  refers to the distribution of the distances between  $\omega$  and the other elements of  $\Omega$ . Depth profiles can be harnessed to define *transport ranks*, which capture the centrality of each element in  $\Omega$  with respect to the entire data cloud based on the optimal transport maps between the depth profiles. We study the properties of transport ranks and show that they provide an effective device for detecting and visualizing patterns in samples of random objects. Specifically, we study estimates of depth profiles and transport ranks based on samples of random objects and establish the convergence of the empirical estimates to the population targets using empirical process theory. We demonstrate the usefulness of depth profiles and associated transport ranks and visualizations for distributional data through a sample of age-at-death distributions for various countries, for compositional data through energy usage for U.S. states and for network data through New York taxi trips.

*Keywords:* Metric space valued data; transport rank; outlyingness; visualization of random objects; Wasserstein metric; empirical process

---

<sup>\*</sup>Contributed equally to the paper.

<sup>†</sup>Research supported in part by NSF grant DMS-2014626

## 1 Introduction

Substantial efforts have been made to describe the center-outward ordering of data. While it is straightforward for univariate measurements, developing such a measure is challenging for multivariate data due to the lack of total ordering in  $\mathbb{R}^p$  for  $p > 1$ , not to speak of random objects, which refer to data that take values in general metric spaces. Statistical depth has emerged as the main device to determine the centrality of multivariate data with respect to an underlying probability distribution, and has a long history and rich literature including halfspace depth (Tukey 1975), convex hull peeling depth (Barnett 1976), simplicial volume depth (Oja 1983), simplicial depth (Liu 1990), zonoid depth (Koshevoy and Mosler 1997), projection depth (Zuo and Serfling 2000), and spatial depth (Serfling 2002), as well as families of depths (Paindaveine and Van Bever 2013; Yang and Modarres 2018), with a recent review in Mosler and Mozharovskyi (2021).

Choosing among different notions of depths, Zuo and Serfling (2000) and Dyckerhoff (2004) discussed two sets of desirable postulates regarding invariance, monotonicity, continuity and convexity; see Mosler (2013) for a more recent discussion. Consequently, depths constitute a versatile tool for descriptive and inferential statistics that has been employed, for example, in quantification of outlyingness and deepest points, data visualization, regression, classification, clustering and testing (Liu et al. 1999; Rousseeuw et al. 1999; Rousseeuw and Hubert 1999; Jörnsten 2004; Li and Liu 2004; Ghosh and Chaudhuri 2005; Li et al. 2012; Liu et al. 2013; Lange et al. 2014, among others).

Notions of depths have also met with growing popularity in the analysis of functional data that consist of random functions. Various definitions of depths have been proposed for functional data that include two major classes of depths (Mosler and Mozharovskyi 2021), integrated depths (Nagy et al. 2016) and infimal depths (Mosler and Polyakova 2012; Mosler 2013). Integrated depths include integrals of cross-sectional univariate depths (Fraiman and Muniz 2001), modified band depth (López-Pintado and Romo 2009), modified half-region depth (López-Pintado and Romo 2011) and multivariate functional integrated depths (Claeskens et al. 2014), while depths of infimal type include band depth (López-Pintado and Romo 2009), functional Tukey depth (Dutta et al. 2011), and half-region depth (López-Pintado and Romo 2011). We refer to Gijbels and Nagy (2017)

for a comprehensive review and discussion of functional depths and their desirable properties; see also [Nieto-Reyes and Battey \(2016\)](#).

In this paper we go beyond multivariate and functional data, which are usually viewed as random elements taking values in a vector space, and consider more complex data that we refer to as random objects. Random objects reside in a space equipped with a metric or dissimilarity measure, which generally lacks a linear structure and is not a vector space. These include data on finite- and infinite-dimensional manifolds such as the Wasserstein space of distributions or data in general Hadamard spaces ([Lin and Müller 2021](#)). Such data are increasingly becoming available in the course of the evolving framework of data science. Notions of depths have been generalized to data lying in a finite-dimensional manifold, including circular and spherical data ([Liu and Singh 1992](#)), covariance or correlation matrices ([Zhang 2002](#); [Chen et al. 2018](#); [Paindaveine and Van Bever 2018](#)) and Hermitian positive definite matrices ([Chau et al. 2019](#)). Lens depth, which is based on the notion of distance, was first introduced in multivariate settings ([Liu and Modarres 2011](#)) and has recently been extended to data taking values in Riemannian manifolds and semimetric/metric spaces ([Kleindessner and von Luxburg 2017](#); [Cholaquidis et al. 2020](#); [Geenens et al. 2021](#)). Other very recent parallel developments which appeared on arXiv while this article was finalized include an extension of Tukey’s depth to the case of random objects ([Dai and Lopez-Pintado 2021](#)) and an approach to nonparametric inference in metric spaces using a distributional approach ([Wang et al. 2021](#)), extending recent work on ball distance correlation ([Pan et al. 2020](#)).

Exploring the geometry of random objects as shaped by the underlying metric  $d$  is crucial for modern data science applications. Our primary goal is thus to develop a toolbox for this purpose. It turns out that these tools can be harnessed to obtain a notion of data depth that differs substantially from existing notions of depth and thus offers a new perspective. Previous approaches that focused on depth for data that are either not finite-dimensional or do not reside in a linear space adopted classical notions of depth for multivariate data as a starting point, then extending them to more general spaces in various ways. In contrast, from the get-go we develop tools directly aimed at random objects in metric spaces; the key notion of transport depth has so far not been considered even for classical structured linear spaces. Our starting point are depth

profiles for each element in the space  $\Omega$  that lend themselves to visualize random objects and in combination with optimal transport quantify centrality and outlyingness. Depth profiles emerge as basic tools for the exploratory analysis of samples of random objects. Our methods are grounded in principled modeling and supported by theory. We develop sample based estimators of the proposed notions of depth profiles, transport ranks and transport medians and establish their convergence to the corresponding population targets. For the theory challenges arise from both the nonlinearity of the underlying metric space and from the fact that the estimated depth profiles are not independent. We overcome these challenges by employing tools from empirical processes.

The *depth profiles* that are key to our approach are indexed by the elements  $\omega \in \Omega$ . Given  $\omega$ , the depth profile at  $\omega$  is the distribution of the distances between  $\omega$  and the other elements of  $\Omega$ , where this distribution is determined by the probability measure on  $\Omega$  that governs the distribution of the random objects across  $\Omega$  and generates the observed data. The depth profile thus associates a one-dimensional distribution to each  $\omega \in \Omega$ . Depth profiles indicate the relative location of  $\omega$  within  $\Omega$ , and for the case of a data sample the relative location of  $\omega$  within the data point cloud of random objects. A second key idea is to harness optimal transports between the distributions that constitute the depth profiles at different elements  $\omega$ . These optimal transports then lead to the definition of a *transport rank* that constitutes a notion of depth and provides an outwards ordering for random objects. We will show that transport ranks can also be used to identify the most central random objects, the *transport median set*.

In Section 2, we introduce the key ingredients of our methodology, i.e. depth profiles, transport ranks and transport median sets. In Section 3, we describe their properties and fundamental features, for example, invariance under measure preserving and distance preserving maps. We propose sample based estimators and establish asymptotic guarantees in Section 4 and then proceed to illustrate the efficacy and visualization of depth profiles and transport ranks with simulated multivariate and distribution-valued data in Section 5. The potential of the new notions for data science will be demonstrated through data applications in Section 6, featuring human mortality distributions, U.S. electricity generation compositions, and Manhattan Yellow Taxi trip records. Proofs and auxiliary results are in the Supplement.

## 2 Depth Profiles, Transport Ranks and Transport Median Set

In this section we introduce and motivate the key notions for our approach. We assume that data and random objects of interest are situated in a totally bounded separable metric space  $(\Omega, d)$ . Consider a probability space  $(S, \mathcal{S}, \mathbb{P})$ , where  $\mathcal{S}$  is the Borel sigma algebra on a domain  $S$  and  $\mathbb{P}$  is a probability measure. A random object  $X$  is a measurable map,  $X: S \rightarrow \Omega$  and  $P$  is a Borel probability measure that generates the law of  $X$ , i.e.  $P(A) = \mathbb{P}(\{s \in S : X(s) \in A\}) =: \mathbb{P}(X \in A) = \mathbb{P}(X^{-1}(A)) =: \mathbb{P}X^{-1}(A)$ , for any Borel measurable  $A \subseteq \Omega$ . For any  $\omega \in \Omega$ , let  $F_\omega$  denote the cumulative distribution function (cdf) of the distribution of the distance between  $\omega$  and a random element  $X$  that is distributed according to  $P$ . We suppress the dependence of  $F_\omega$  on  $P$  to keep the notation simple.

Formally, for any  $t \in \mathbb{R}$ , we define the *depth profile* at  $\omega$  as

$$F_\omega(t) = \mathbb{P}(d(\omega, X) \leq t), \quad (1)$$

so that  $F_\omega$  is a one-dimensional distribution that captures the probability masses enclosed by a ball in  $\Omega$  that has center  $\omega$  and radius  $t$ , for all  $t \geq 0$ . Another interpretation is that the depth profile at  $\omega$  is the distribution of the distances that need to be covered to reach other elements of  $\Omega$  when starting out at  $\omega$ , as dictated by the distribution  $P$  of random elements  $X$  that take values in  $\Omega$ . An element  $\omega$  that is centrally located, i.e. close to most other elements, will have a density profile with more mass near 0, in contrast to a distantly located or outlying element whose depth profile will assign mass farther away from 0. If depth profiles have densities, for a centrally located  $\omega$ , this density will have a mode near 0, while the density near 0 will be small for a distantly located  $\omega$ .

A central notion will be the  $\omega$ -indexed stochastic process  $\{d(\omega, X)\}_{\omega \in \Omega}$ . For each  $k \in \mathbb{N}$  and collection of indices  $i_1, i_2, \dots, i_k$ , we consider the  $\mathbb{R}^k$  valued random variable  $(d(\omega_{i_1}, X), d(\omega_{i_2}, X), \dots, d(\omega_{i_k}, X))$  defining a probability measure  $Q_{i_1, i_2, \dots, i_k}$  such that

$$Q_{i_1, i_2, \dots, i_k}(A_1 \times A_2 \times \dots \times A_k) := \mathbb{P}(d(\omega_{i_1}, X) \in A_1, d(\omega_{i_2}, X) \in A_2, \dots, d(\omega_{i_k}, X) \in A_k)$$

for any Borel sets  $A_1, A_2, \dots, A_k \subseteq \mathbb{R}$ . Suppose that  $Q_{i_1, i_2, \dots, i_k}$  satisfies the following conditions:

(i) for any permutation  $\pi = (\pi(1), \dots, \pi(k))$  of  $\{1, \dots, k\}$  and measurable sets  $A_j \subseteq \mathbb{R}$ ,

$$Q_{\pi(i_1), \pi(i_2), \dots, \pi(i_k)}(A_{\pi(1)} \times A_{\pi(2)} \times \dots \times A_{\pi(k)}) = Q_{i_1, i_2, \dots, i_k}(A_1 \times A_2 \times \dots \times A_k).$$

(ii) for all measurable sets  $A_j \subseteq \mathbb{R}$  and for any  $m \in \mathbb{N}$

$$\begin{aligned} & Q_{i_1, i_2, \dots, i_k}(A_1 \times A_2 \times \dots \times A_k) \\ &= Q_{i_1, i_2, \dots, i_k, i_{k+1}, \dots, i_{k+m}}(A_1 \times A_2 \times \dots \times A_k \times \mathbb{R} \times \dots \times \mathbb{R}). \end{aligned}$$

Then by Kolmogorov's extension theorem, there exists a unique probability measure  $\nu$  on  $\mathbb{R}^\Omega := \{\omega \mapsto g(\omega) : \omega \in \Omega, g(\omega) \in \mathbb{R}\}$ , the underlying law of the stochastic process  $\{d(\omega, X)\}_{\omega \in \Omega}$ , whose finite dimensional marginals are given by  $Q_{i_1, i_2, \dots, i_k}$ , whence the stochastic process  $\{d(\omega, X)\}_{\omega \in \Omega}$  is well defined.

For  $\omega \in \Omega$  and  $r > 0$ , define the open ball  $O_{\omega, r} = \{x \in \Omega : d(\omega, x) < r\}$  with radius  $r$  centered at  $\omega$ . Starting with the open balls  $\{O_{\omega, r}\}_{\omega \in \Omega, r > 0}$ , we form an algebra  $\mathcal{B}_0$  of subsets of  $\Omega$ , which includes the empty set and open balls and is closed under complements, finite unions and finite intersections. On  $\mathcal{B}_0$ , we define a pre-measure  $P_0$ , given by the marginals of the law of  $\{d(\omega, X)\}_{\omega \in \Omega}$  such that  $P_0(B) = P(B) = \mathbb{P}(X^{-1}(B))$  for all  $B \in \mathcal{B}_0$ . When  $\Omega$  is separable,  $\mathcal{B}_0$  generates the Borel sigma algebra on  $\Omega$  since it is an algebra containing the open balls. Hence by the Hahn–Kolmogorov theorem, a version of the Carathéodory's extension theorem, there exists a unique extension of  $P_0$  to the Borel sigma algebra of  $\Omega$  whose restriction to  $\mathcal{B}_0$  coincides with  $P_0$ . By uniqueness, the extension of  $P_0$  is  $P$ . Hence the marginals of the law of  $\{d(\omega, X)\}_{\omega \in \Omega}$  uniquely characterize the underlying Borel probability measure of  $X$  on separable metric spaces.

The collection of depth profiles  $\{F_\omega : \omega \in \Omega\}$  represents the one-dimensional marginals of the stochastic process  $\{d(\omega, X)\}_{\omega \in \Omega}$ . Our goal is to use these simple marginals to obtain information about the very complex distribution of the  $\Omega$ -valued random variable  $X$ . The empirical versions of these marginals are the estimated depth profiles introduced below that we utilize to explore the

geometry of point clouds of random objects.

Considering the depth profile  $F_X$  of  $X$ , for each  $\omega$ , the push-forward map of  $F_\omega$  to  $F_X$ , given by  $F_X^{-1}(F_\omega(\cdot))$ , outlines the shape of the optimal transport from the depth profile  $F_\omega$  to the depth profile  $F_X$ . We will use the optimal transport map subtracted by the identity map (Ambrosio et al. 2008),

$$H_{X,\omega}(u) = F_X^{-1}(F_\omega(u)) - u, \quad u \geq 0, \quad (2)$$

to assign a measure of centrality to an element  $\omega \in \Omega$  with respect to  $P$ . When  $F_\omega$  is continuous, by change of variable, the integral

$$\int |H_{X,\omega}(u)| dF_\omega(u) = \int_0^1 |F_X^{-1}(u) - F_\omega^{-1}(u)| du \quad (3)$$

quantifies the amount of mass that needs to be transferred when transporting  $F_\omega$  to  $F_X$ ;

$$\text{sign} \left( \int H_{X,\omega}(u) dF_\omega(u) \right) = \text{sign} \left( \int_0^1 [F_X^{-1}(u) - F_\omega^{-1}(u)] du \right) \quad (4)$$

summarizes overall the direction of mass transfer, either from right to left in which case the sign is negative, or from left to right when it is positive.

The intuition about the utility of these notions is that if  $\omega$  is more centrally located than  $X$  in regard to the measure  $P$ , we expect the sign to be positive as the mass transfer is predominantly from left to right and the amount of transferred mass to reflect the outlyingness differential between  $\omega$  and  $X$ . For example, for distributions  $P$  that are symmetric around and declining as moving away from a central point  $\omega_\oplus \in \Omega$ , we expect that the sign in (4) with  $\omega = \omega_\oplus$  is positive almost surely and that given  $X$ , the amount of mass transfer is increasing as  $d(\omega_\oplus, X)$  increases. To determine the degree of centrality or outlyingness it makes therefore sense to take the expected value of the mass transferred for a random  $X$ , calibrated by the sign indicating the transfer direction. This is illustrated in Figure 1 for the case where  $X$  is a bivariate Gaussian random variable with mean zero and covariance  $\text{diag}(2, 1)$ . For  $x \in \{(0, 0), (2, 0), (4, 0), (6, 0)\}$  and  $\omega = (2, 2)$ , their corresponding

depth profiles are depicted as densities  $f_x$  and  $f_\omega$  in the left panel, where the distances from  $x$  to the rest of the data are increasing as  $x$  moves away from the origin. For  $x \in \{(0,0), (2,0), (4,0), (6,0)\}$ , the maps  $H_{x,\omega}$  as per (2) to a fixed element  $\omega = (2,2)$  are in the right panel. For  $\omega = (2,2)$ , mass moves to the left when transporting  $F_\omega$  to  $F_x$  for  $x \in \{(0,0), (2,0)\}$ , which are closer to the origin, and moves to the right for  $x \in \{(4,0), (6,0)\}$ , which are farther away from the origin.

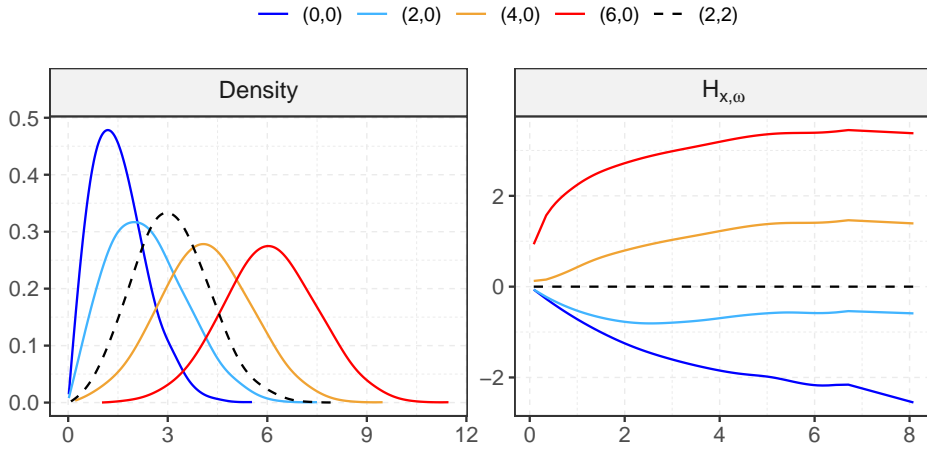


Figure 1: Left: Depth profiles, represented by the corresponding densities, of five points as indicated, with respect to a bivariate Gaussian distribution with mean zero and covariance  $\text{diag}(2, 1)$ . Right: Transport maps  $H_{x,\omega}$  as per (2) for  $x \in \{(0,0), (2,0), (4,0), (6,0)\}$  and  $\omega = (2,2)$ , where negative (positive) values indicate transport to the right (left).

This motivates *transport ranks* to measure centrality (which can be viewed as a notion of depth) of an element  $\omega \in \Omega$  with respect to  $P$  as the expected signed amount of mass transfer when transporting  $F_\omega$  to  $F_X$ , where  $P = \mathbb{P}X^{-1}$ . Formally,

$$R_\omega = \mathbb{E} \left\{ \text{sign} \left( \int_0^1 [F_X^{-1}(u) - F_\omega^{-1}(u)] du \right) \int_0^1 |F_X^{-1}(u) - F_\omega^{-1}(u)| du \right\}. \quad (5)$$

Given a sample of independent observations  $X_1, \dots, X_n$  from  $P$ , we define a pairwise comparison graph  $\mathcal{V}$ , where

$$\mathcal{V}_{ij} = \left\{ \text{sign} \left( \int_0^1 [F_{X_i}^{-1}(u) - F_{X_j}^{-1}(u)] du \right) \int_0^1 |F_{X_i}^{-1}(u) - F_{X_j}^{-1}(u)| du \right\}, \quad 1 \leq i, j \leq n, \quad (6)$$

and  $\mathcal{V}_{ij}$  expresses a relative order of centrality between pairs  $X_i$  and  $X_j$  by using their depth profiles

$F_{X_i}$  and  $F_{X_j}$ , where  $X_i$  is more central than  $X_j$  if  $\mathcal{V}_{ij} < 0$  and  $X_j$  is more central than  $X_i$  if  $\mathcal{V}_{ij} > 0$ , and the size of the difference in centrality is indicated by  $|\mathcal{V}_{ij}|$ . This is similar to the notion of *HodgeRank* (Jiang et al. 2011). The matrix  $\mathcal{V}$  is skew symmetric. The empirical transport rank of  $X_i$ , with regard to the empirical measure corresponding to  $\{X_1, \dots, X_n\}$ , is given by

$$\mathbb{E}_{X_j} \left( \left\{ \text{sign} \left( \int_0^1 [F_{X_i}^{-1}(u) - F_{X_j}^{-1}(u)] du \right) \int_0^1 |F_{X_i}^{-1}(u) - F_{X_j}^{-1}(u)| du \right\} \right). \quad (7)$$

It expresses the aggregated preference of  $X_i$  with respect to the rest of the data cloud. The more positive the transport rank of  $X_i$  is, the more centered it is relative to the other sample elements, because the optimal transports from  $X_i$  to the other points in the data cloud tend to move mass to the right.

Equipped with an ordering of the elements of  $\Omega$  by means of their transport rank we define the *transport median* set of  $P$  as the collection of points in the support  $\Omega_P \subset \Omega$  of  $P$  which have maximal transport rank and are therefore most central. Formally, the transport median set  $\mathcal{M}_\oplus$  is defined as

$$\mathcal{M}_\oplus = \underset{\omega \in \Omega_P}{\text{argmax}} R_\omega. \quad (8)$$

The depth profiles of the data objects together with the transport ranks and the transport median set are the key ingredients of the proposed toolkit and notion of centrality for the exploration of samples of random objects. These devices lend themselves to devise depth profile based methods for clustering, classification and outlier detection, all challenging tasks when one deals with random objects.

### 3 Properties of Depth Profiles and Transport Ranks

We discuss here some desirable properties of depth profiles, transport ranks and the transport median set. By Lemma 1 established in Section 4 under Assumption (A2), the depth profiles  $F_\omega(\cdot)$  and the associated quantile function representations  $F_\omega^{-1}(\cdot)$  are uniformly Lipschitz in  $\omega$  provided that the depth profiles have uniformly upper bounded densities with respect to the Lebesgue measure.

This means that  $F_{\omega_1}$  and  $F_{\omega_2}$  are uniformly close to each other as long as  $\omega_1$  and  $\omega_2$  are close, and the distance between  $F_{\omega_1}$  and  $F_{\omega_2}$  is upper bounded by a constant factor of  $d(\omega_1, \omega_2)$ . Moreover, under the well-separateness Assumption (A3) in Section 4 the transport rank  $R_\omega$  is uniformly continuous in  $\omega$  as shown in Lemma 2. Let  $(\tilde{\Omega}, \tilde{d})$  be a metric space. A map  $h: \Omega \rightarrow \tilde{\Omega}$  is isometric if  $d(\omega_1, \omega_2) = \tilde{d}(h(\omega_1), h(\omega_2))$  for all  $\omega_1, \omega_2 \in \Omega$ . Proposition 1(a) below establishes the invariance of the depth profiles, and thereby the transport rank, under isometric transformations. In Euclidean spaces this ensures that the depth profiles are invariant under affine transformations and rotations.

Next we consider situations when the distribution  $P$  of  $X$  concentrates around a point  $\omega_\oplus \in \Omega$ , specifically, when there exists  $\omega_\oplus \in \Omega$  such that  $d(\omega_\oplus, \omega_1) \leq d(\omega_\oplus, \omega_2)$  implies

$$F_{\omega_1}(u) \geq F_{\omega_2}(u) \tag{9}$$

for  $u$  almost everywhere in  $\mathbb{R}$ , with a strict inequality  $d(\omega_\oplus, \omega_1) < d(\omega_\oplus, \omega_2)$  implying that  $F_{\omega_1}(u) > F_{\omega_2}(u)$  on a set with positive Lebesgue measure. We call such  $\omega_\oplus$  an  $\Omega$ -valued *mode* of  $P$ . Note that the definition of modes implies the uniqueness of  $\omega_\oplus$ . This condition says that a  $d$ -ball of radius  $u$  around  $\omega_\oplus$  contains more mass under  $P$  than a similar ball around any other point in  $\Omega$  and the mass contained around a point  $\omega$  decreases as distance from  $\omega_\oplus$  increases. In the above definition, if for any two points  $\omega_1, \omega_2$ ,  $F_{\omega_1}(u) = F_{\omega_2}(u)$  almost everywhere under the Lebesgue measure, then  $d(\omega_\oplus, \omega_1) = d(\omega_\oplus, \omega_2)$ , which implies that the mode  $\omega_\oplus$ , if it exists, is unique. Proposition 1(b) states that if  $P$  has a mode, then the transport rank of the mode is positive and the transport median is unique and corresponds to the mode. In fact the transport rank decreases as the distance from the mode increases and stays constant for all  $\omega$  which are equidistant from  $\omega_\oplus$ . For distributions that concentrate around their unique Fréchet mean (Fréchet 1948), the Fréchet mean is the mode and hence the transport median (Lunagómez et al. 2020).

**Proposition 1.** *For a separable metric space  $(\Omega, d)$  the depth profiles  $F_\omega$  and the transport ranks  $R_\omega$  satisfy the following properties*

- (a) *Let  $h: \Omega \rightarrow \tilde{\Omega}$  be a bijective isometric measurable map between  $(\Omega, d)$  and  $(\tilde{\Omega}, \tilde{d})$  and  $P_h(\cdot) = P(h^{-1}(\cdot))$  the push-forward measure on  $\tilde{\Omega}$ . Then  $F_{h(\omega)}^{P_h}(u) = F_\omega^P(u)$  for all  $u \in \mathbb{R}$ , and hence*

$R_{h(\omega)}^{P_h} = R_\omega^P$ . Here,  $F_\omega^P(u) = \mathbb{P}(d(\omega, X) \leq u)$ , where  $X$  is a  $\Omega$ -valued random element such that  $P = \mathbb{P}X^{-1}$  (and hence  $P_h = \mathbb{P}(h(X))^{-1}$ ),  $F_{h(\omega)}^{P_h}(u) = \mathbb{P}(\tilde{d}(h(\omega), h(X)) \leq u)$ ,  $R_\omega^P$  is the transport rank of  $\omega$  with respect to  $P$  and  $R_{h(\omega)}^{P_h}$  is the transport rank of  $h(\omega)$  with respect to  $P_h$ .

(b) Let  $\omega_+$  be a mode as per (9) of  $P$ . Then  $R_{\omega_+} \geq 0$  and  $R_\omega$  is a non-increasing function of  $d(\omega_+, \omega)$ . Moreover  $R_{\omega_1} = R_{\omega_2}$  if  $d(\omega_+, \omega_1) = d(\omega_+, \omega_2)$ . Hence for such  $P$  the transport median  $\mathcal{M}_+$  is unique and  $\mathcal{M}_+ = \omega_+$ .

Proposition 1(b) provides a characterization of the radial ordering induced by the transport rank for the special case where the data distribution on  $\Omega$  has a mode.

Consider a curve  $\gamma: I \rightarrow \Omega$  in the space  $(\Omega, d)$  where  $I \subset \mathbb{R}$  is a non-empty interval. The length of the curve  $L(\gamma)$  is defined as

$$L(\gamma) = \sup \sum_{i=1}^k d(\gamma(t_i), \gamma(t_{i-1})), \quad (10)$$

where the supremum in (10) is taken over all  $t_0 \leq t_1 \leq \dots \leq t_k$  in  $I$  and all  $k \in \mathbb{N}$ ;  $\gamma$  is called a rectifiable curve if  $L(\gamma) < \infty$ . A length metric  $d_L$  associated with the metric  $d$  of  $\Omega$  is then

$$d_L(x, y) = \inf_{\gamma \in \mathcal{L}} L(\gamma), \quad (11)$$

where the infimum in (11) is taken over the class of curves  $\mathcal{L} = \{\gamma: [0, 1] \rightarrow \Omega \mid \gamma(0) = x, \gamma(1) = y, \text{ and } \gamma \text{ is rectifiable}\}$ . Then  $(\Omega, d)$  is a length space if  $d(x, y) = d_L(x, y)$  for all  $x, y \in \Omega$ . A curve  $\gamma: I \rightarrow \Omega$  has constant speed if there exists  $\lambda > 0$ , the speed of  $\gamma$ , such that  $L(\gamma|_{[t, t']}) = \lambda|t - t'|$  for all  $t \leq t'$  contained in  $I$ . A constant speed curve  $\gamma$  is a geodesic if  $L(\gamma|_{[t, t']}) = d(\gamma(t), \gamma(t')) = \lambda|t - t'|$  for all  $t \leq t'$  contained in  $I$ , and  $(\Omega, d)$  is a geodesic space if for all pairs of points  $x, y \in \Omega$ , there exists a geodesic  $\gamma: [0, 1] \rightarrow \Omega$  such that  $\gamma(0) = x$  and  $\gamma(1) = y$ . Corollary 1 shows the monotonicity of the transport rank along geodesics starting from a mode when  $\Omega$  is a geodesic space.

**Corollary 1.** Let  $(\Omega, d)$  be a geodesic space and  $P$  a distribution on  $\Omega$  such that  $\omega_+$  is the mode of  $P$ . Let  $\gamma: [0, 1] \rightarrow \Omega$  be a geodesic such that  $\gamma(0) = \omega_+$  and  $d_L(\gamma(0), \gamma(1)) = d(\gamma(0), \gamma(1))$ . Then

for any  $t, t' \in [0, 1]$  such that  $t \leq t'$ ,  $R_{\gamma(t)} \leq R_{\gamma(t')}$  with strict inequality if  $t < t'$ .

The set of maximizers of  $R_\omega$  in  $\Omega_P$  constitutes the transport median set defined in (8). The function  $R_\omega$  is uniformly continuous under Assumption (A3). Therefore when (A3) holds, the transport median set is guaranteed to be non-empty whenever  $\Omega_P$  is compact. If  $\Omega$  is a length space which is complete and locally compact, then by the Hopf–Rinow theorem,  $\Omega$  is a geodesic space, and if  $\Omega_P$  is any bounded closed subset of  $\Omega$ , then it is guaranteed to be compact.

Equipped with an ordering of the elements of  $\Omega$  in terms of their transport ranks, it is natural to consider level sets of the form  $L_\alpha = \{\omega \in \Omega : R_\omega = \alpha\}$  and nested superlevel sets  $L_\alpha^+ = \{\omega \in \Omega : R_\omega \geq \alpha\}$ . By definition,  $L_{\alpha_1}^+ \subseteq L_{\alpha_2}^+$  whenever  $\alpha_1 \geq \alpha_2$ . By the continuity of  $R_\omega$  under Assumption (A3) the sets  $L_\alpha$  and  $L_\alpha^+$  are closed. Moreover when  $(\Omega, d)$  is a bounded, complete and locally compact length space, by the Hopf–Rinow theorem  $L_\alpha$  and  $L_\alpha^+$  are compact as well. There are numerous important applications of level sets and superlevel sets of random objects, for example superlevel sets  $L_\alpha^+$  can be viewed as depth regions and level sets can be used to define *depth quantile sets*. These can be viewed as a generalization of univariate quantiles to the case of random objects. Specifically, a  $\zeta$ -level depth quantile set can be defined as  $L_\alpha$  such that  $P(X \in L_\alpha^+) = \zeta$ , for  $\zeta \in (0, 1)$ . Complements of superlevel sets can be used to identify potential outliers by highlighting observations with low transport ranks and can be also employed for data trimming by excluding points which have transport ranks lower than a threshold  $\alpha$ ; one then might consider maximizers of  $R_\omega$  over trimmed versions of  $\Omega_P$  to obtain trimmed analogues of the transport median set  $\mathcal{M}_\oplus$ .

## 4 Estimation and Theory

While so far we have introduced the notions of profile depth, transport rank and transport median sets at the population level, in practice one needs to estimate these quantities from a data sample of random objects  $\{X_i\}_{i=1}^n$ , i.e. a sample of  $n$  independent realizations of  $X$ . For estimating the depth profiles  $F_\omega$ ,  $\omega \in \Omega_P$ , we consider the empirical estimates

$$\widehat{F}_\omega(t) = \frac{1}{n} \sum_{i=1}^n \mathbb{I}\{d(\omega, X_i) \leq t\}, \quad t \in \mathbb{R}. \quad (12)$$

Replacing expectations with empirical means and using estimated depth profiles  $\widehat{F}_{X_i}$  as surrogates of  $F_{X_i}$ , we obtain estimates for the transport  $\omega \in \Omega$  defined in (5) as

$$\widehat{R}_\omega = \frac{1}{n} \sum_{i=1}^n \text{sign} \left( \int_0^1 [\widehat{F}_{X_i}^{-1}(u) - \widehat{F}_\omega^{-1}(u)] du \right) \int_0^1 |\widehat{F}_{X_i}^{-1}(u) - \widehat{F}_\omega^{-1}(u)| du. \quad (13)$$

The term  $\int_0^1 |\widehat{F}_{X_i}^{-1}(u) - \widehat{F}_\omega^{-1}(u)| du$  quantifies the discrepancy between  $\widehat{F}_{X_i}$  and  $\widehat{F}_\omega$ , while the sign of  $\int_0^1 [\widehat{F}_{X_i}^{-1}(u) - \widehat{F}_\omega^{-1}(u)] du$  provides a comparison of the outlyingness of  $\omega$  and  $X_i$ ; a positive or negative sign indicates that  $\omega$  is more central or outlying than  $X_i$ , respectively. Finally we define the estimated transport median set  $\widehat{\mathcal{M}}_\oplus$  as

$$\widehat{\mathcal{M}}_\oplus = \underset{\omega \in \{X_1, X_2, \dots, X_n\}}{\text{argmax}} \widehat{R}_\omega.$$

To obtain asymptotic properties of these estimators and convergence towards their population targets, we require the following assumptions.

(A1) Let  $N(\varepsilon, \Omega, d)$  be the covering number of the space  $\Omega$  with balls of radius  $\varepsilon$  and  $\log N(\varepsilon, \Omega, d)$  the corresponding metric entropy, which satisfies

$$\varepsilon \log N(\varepsilon, \Omega, d) \rightarrow 0 \quad \text{as} \quad \varepsilon \rightarrow 0. \quad (14)$$

(A2) For every  $\omega \in \Omega$  assume that  $F_\omega$  is absolutely continuous with continuous density  $f_\omega$  and let  $\underline{\Delta}_\omega = \inf_{t \in \text{supp}(f_\omega)} f_\omega(t)$  and  $\overline{\Delta}_\omega = \sup_{t \in \mathbb{R}} f_\omega(t)$ . Assume that  $\underline{\Delta}_\omega > 0$  for each  $\omega \in \Omega$ . Moreover assume there exists  $\overline{\Delta} > 0$  such that

$$\sup_{\omega \in \Omega} \overline{\Delta}_\omega \leq \overline{\Delta}.$$

(A3) For some  $\eta, K > 0$  and for all  $0 < \varepsilon < \eta$ , there exists  $\tau(\varepsilon) > K\varepsilon$  such that

$$\inf_{d(\omega_1, \omega_2) > \varepsilon} \left| \int_0^1 F_{\omega_1}^{-1}(u) du - \int_0^1 F_{\omega_2}^{-1}(u) du \right| \geq \tau(\varepsilon).$$

(A4) For some  $\eta' > 0$ , for any  $0 < \varepsilon < \eta'$ ,  $\alpha(\varepsilon) = \inf_{\omega_{\oplus} \in \mathcal{M}_{\oplus}} \inf_{d(\omega, \omega_{\oplus}) > \varepsilon} |R_{\omega} - R_{\omega_{\oplus}}| > 0$ .

Assumptions (A1) and (A2) are necessary for Theorem 1 which provides the uniform convergence of  $\widehat{F}_{\omega}$  to  $F_{\omega}$ . This is the primary device to overcome the dependence between the summands in the estimator of the transport rank and to establish its uniform convergence to the population transport rank. For any  $t \in \mathbb{R}$ ,  $F_{\omega}(t) = \mathbb{E}(\widehat{F}_{\omega}(t))$ . We define functions  $y_{\omega, t}(x) = \mathbb{I}\{d(\omega, x) \leq t\} : \Omega \rightarrow \mathbb{R}$  and the function class  $\mathcal{F} = \{y_{\omega, t} : \omega \in \Omega, t \in \mathbb{R}\}$ . Theorem 1 establishes that under assumptions (A1) and (A2) the function class  $\mathcal{F}$  is  $P$ -Donsker.

**Theorem 1.** *Under assumptions (A1) and (A2),  $\{\sqrt{n}(\widehat{F}_{\omega}(t) - F_{\omega}(t)) : \omega \in \Omega, t \in \mathbb{R}\}$  converges weakly to a zero-mean Gaussian Process  $\mathbb{G}_P$  with covariance given by*

$$\mathcal{C}_{(\omega_1, t_1), (\omega_2, t_2)} = \text{Cov}(y_{\omega_1, t_1}(X) y_{\omega_2, t_2}(X)).$$

Assumption (A1) is a restriction on the complexity of the metric space  $(\Omega, d)$  which is satisfied for a broad class of spaces. Assumption (A2) is a mild regularity condition on the depth profiles. Assumption (A3) guarantees that in a small neighborhood of any  $\omega \in \Omega$ , the ‘‘expectations’’ of the depth profiles, i.e.  $\int_0^1 F_{\omega}^{-1}(u)du = \int_0^1 u f_{\omega}(u)du$  are well separated. Assumption (A4), which is needed primarily to guarantee convergence of the estimated transport median set  $\widehat{\mathcal{M}}_{\oplus}$ , guarantees that the transport ranks of points outside of  $\varepsilon$ -neighbourhoods of any  $\omega_{\oplus} \in \mathcal{M}_{\oplus}$  are well separated from  $R_{\omega_{\oplus}}$  as long as  $\varepsilon$  is small enough.

Any space  $(\Omega, d)$  such that  $\log N(\varepsilon, \Omega, d) = O\left(\frac{1}{\varepsilon^{\alpha}}\right)$  for some  $\alpha < 1$  satisfies Assumption (A1). This is true for any  $(\Omega, d)$  which can be represented as a subset of elements in a finite dimensional Euclidean space, for example the space of graph Laplacians or network adjacency matrices with fixed number of nodes (Kolaczyk et al. 2020; Ginestet et al. 2017), SPD matrices of a fixed size (Dryden et al. 2009; Thanwerdas and Pennec 2021), simplex valued objects in a fixed dimension (Jeon and Park 2020; Chen et al. 2012) and the space of phylogenetic trees with the same number of tips (Kim et al. 2020; Billera et al. 2001). It holds that  $\log N(\varepsilon, \Omega, d) = O(\varepsilon^{-\alpha})$  for any  $\alpha < 1$  when  $\Omega$  is a VC-class of sets or a VC-class of functions (Theorems 2.6.4 and 2.6.7, van der Vaart and Wellner 1996). Assumption (A1) holds for  $p$ -dimensional smooth function classes  $C_1^{\alpha}(\mathcal{X})$  (page 155,

van der Vaart and Wellner 1996) on bounded convex sets  $\mathcal{X}$  in  $\mathbb{R}^p$  equipped with the  $\|\cdot\|_\infty$ -norm (Theorem 2.7.1, van der Vaart and Wellner 1996) and  $\|\cdot\|_{r,Q}$ -norm which is the  $L_r(Q)$  for any probability measure  $Q$  on  $\mathbb{R}^p$  (Corollary 2.7.2, van der Vaart and Wellner 1996), if  $\alpha \geq p + 1$ .

Of particular interest for many applications is the case when  $\Omega$  is the space of one-dimensional distributions on some compact interval  $I \subset \mathbb{R}$  with the underlying metric  $d = d_W$  with  $d_W$  being the 2-Wasserstein metric (Petersen et al. 2019), defined in (16). If  $\Omega$  is represented using the quantile function of the distributions then, without any further assumptions,  $\log N(\varepsilon, \Omega, d_W)$  is upper and lower bounded by a factor of  $1/\varepsilon$  (Proposition 2.1, Blei et al. 2007) which does not meet the criterion in (A1). However, if we assume that the distributions in  $\Omega$  are absolutely continuous with respect to the Lebesgue measure on  $I$  with smooth densities uniformly taking values in some interval  $[l_\Omega, u_\Omega]$ , then  $\Omega$  equipped with  $d_W$  satisfies (A1). To see this, observe that with the above characterization of  $\Omega$  the quantile functions corresponding to the distributions in  $\Omega$  have smooth derivatives that are uniformly bounded. If we let  $\mathcal{Q}_{deriv}$  denote the space of the uniformly bounded derivatives of the quantile functions in  $\Omega$ , then  $\log N(\varepsilon, \mathcal{Q}_{deriv}, \|\cdot\|_1) = O(\varepsilon^{-1})$ , where  $\|\cdot\|_1$  is the  $L_1$  norm under the Lebesgue measure on  $I$  (Corollary 2.7.2, van der Vaart and Wellner 1996). Using Lemma 1 in Gao and Wellner (2009), with  $\mathcal{F} \equiv \mathcal{Q}_{deriv}$ ,  $\mathcal{G} \equiv \Omega$ ,  $\alpha(x) = x$  and  $\phi(\varepsilon) = K/\varepsilon$  for some constant  $K$ ,  $\log N(\varepsilon, \Omega, d_W) = O(\varepsilon^{-1/2})$  which meets the requirement of (A1). If  $\Omega$  is the space of  $p$ -dimensional distributions on a compact convex set  $I \subset \mathbb{R}^p$ , represented using their distribution functions endowed with the  $L_r$  metric with respect to the Lebesgue measure on  $I$ , then (A1) is satisfied if  $\Omega \subset C_1^\alpha(I)$  for  $\alpha \geq p + 1$  (see above discussion).

Next we discuss the asymptotic convergence of the estimates  $\hat{R}_\omega$  of transport rank. For this we need Assumption (A3) together with assumptions (A1) and (A2). Theorem 2 establishes a  $\sqrt{n}$ -rate of convergence uniformly in  $\omega$  for  $\hat{R}_\omega$ . The proof of Theorem 2 relies on Corollary 2, which follows from the proof of Theorem 1 and Lemma 1, which shows that the population depth profiles  $F_\omega$  and the corresponding quantile representations  $F_\omega^{-1}$  and  $\hat{F}_\omega^{-1}$  are (almost surely) Lipschitz in  $\omega$ .

**Corollary 2.** *Under assumptions (A1) and (A2),*

$$\sqrt{n} \sup_{\omega \in \Omega} \sup_{u \in [0,1]} \left| \widehat{F}_\omega^{-1}(u) - F_\omega^{-1}(u) \right| = O_{\mathbb{P}}(1).$$

**Lemma 1.** *For any  $\omega_1, \omega_2 \in \Omega$  under Assumption (A2),*

$$\begin{aligned} \sup_{u \in [0,1]} |F_{\omega_1}^{-1}(u) - F_{\omega_2}^{-1}(u)| &\leq d(\omega_1, \omega_2), \\ \sup_{u \in [0,1]} |\widehat{F}_{\omega_1}^{-1}(u) - \widehat{F}_{\omega_2}^{-1}(u)| &\leq d(\omega_1, \omega_2) \text{ (almost surely) and} \\ \sup_{u \in [0,1]} |F_{\omega_1}(u) - F_{\omega_2}(u)| &\leq \overline{\Delta} d(\omega_1, \omega_2). \end{aligned}$$

**Theorem 2.** *Under assumptions (A1)–(A3),*

$$\sqrt{n} \sup_{\omega \in \Omega} |\widehat{R}_\omega - R_\omega| = O_{\mathbb{P}}(1).$$

Next we establish the convergence of the estimated transport median set  $\widehat{\mathcal{M}}_+$  to  $\mathcal{M}_+$ . Define the Hausdorff metric between  $\widehat{\mathcal{M}}_+$  and  $\mathcal{M}_+$  as  $\rho_H(\widehat{\mathcal{M}}_+, \mathcal{M}_+)$  where

$$\rho_H(\widehat{\mathcal{M}}_+, \mathcal{M}_+) = \max \left( \sup_{\omega \in \widehat{\mathcal{M}}_+} d(\omega, \mathcal{M}_+), \sup_{\omega \in \mathcal{M}_+} d(\omega, \widehat{\mathcal{M}}_+) \right) \quad (15)$$

where for any  $\omega \in \Omega$  and any subset  $\mathcal{S} \subset \Omega$ ,  $d(\omega, \mathcal{S}) = \inf_{s \in \mathcal{S}} d(\omega, s)$ . Theorem 3 shows the asymptotic closeness in the Hausdorff metric of the estimated transport median set and the true transport median set. The proof of Theorem 3 relies on assumptions (A1)–(A4) and Lemma 2 that gives local uniform continuity within  $\eta$ -neighborhoods of the transport rank  $R_\omega$  in  $\omega$ .

**Lemma 2.** *Under Assumption (A3), for any  $\omega_1, \omega_2 \in \Omega$  and  $0 < \varepsilon < \eta$ , with  $\eta$  as in Assumption (A3),  $d(\omega_1, \omega_2) < \varepsilon$  implies that*

$$|R_{\omega_1} - R_{\omega_2}| \leq \varepsilon (1 + 2/K)$$

where  $K > 0$  is as in Assumption (A3).

**Theorem 3.** Assume that the distribution  $P$  is such that  $\mathcal{M}_\oplus$  is non-empty. Under assumptions (A1)–(A4),

$$\rho_H(\widehat{\mathcal{M}}_\oplus, \mathcal{M}_\oplus) = o_{\mathbb{P}}(1).$$

## 5 Simulations

For numerical experiments, we perform clustering analysis of the observations  $X_i$  based on their depth profiles  $\widehat{F}_{X_i}$  as per (12) with  $\omega = X_i$ . Note that  $\widehat{F}_{X_i}$  are distributions and hence do not lie in a linear/Euclidean space. Extending  $k$ -means clustering to distribution-valued data, we consider the Wasserstein space  $(\mathcal{W}, d_W)$  of absolute continuous distributions on  $\mathbb{R}$  with finite second moments, where  $d_W$  denotes the Wasserstein metric given by

$$d_W(F_1, F_2) = \left( \int_0^1 [F_1^{-1}(u) - F_2^{-1}(u)]^2 du \right)^{1/2} = d_{L^2}(F_1^{-1}, F_2^{-1}), \text{ for } F_1, F_2 \in \mathcal{W}. \quad (16)$$

Here,  $F_l^{-1}$  denotes the quantile function corresponding to  $F_l$ , for  $l = 1, 2$ ; specifically,  $F_l^{-1}(u) = \inf\{x \in \mathbb{R} : F_l(x) \geq u\}$ , for  $u \in (0, 1)$ . The  $n$  observations are partitioned into  $k$  subsets  $S_1, \dots, S_k$  so as to minimize the within-cluster sums of squared Wasserstein distances,

$$\operatorname{argmin}_{\{S_1, \dots, S_k\}} \sum_{j=1}^k \sum_{i: X_i \in S_j} d_W^2(\widehat{F}_{X_i}, \widehat{F}_{S_j \oplus}), \quad (17)$$

where

$$\widehat{F}_{S_j \oplus} = \operatorname{argmin}_{q \in \mathcal{W}} \sum_{i: X_i \in S_j} d_W^2(\widehat{F}_{X_i}, q) \quad (18)$$

is the empirical Wasserstein barycenter of depth profiles of observations within  $S_j$ , for  $j = 1, \dots, k$ . We refer to this method as  $k$ -W-means clustering. Specifically, numbers of clusters  $k$  are chosen by the minimizer of the ratio between the adjusted between-group sums of squares (BGSS) and within-group sums of squares (WGSS) (Caliński and Harabasz 1974),  $k^* = \operatorname{argmax}_k [\text{BGSS}/(k-1)]/[\text{WGSS}/(n-k)]$ ,

$$\text{WGSS} = \sum_{j=1}^k \frac{1}{|S_j|} \sum_{i < i': X_i, X_{i'} \in S_j} d_W^2(\hat{F}_{X_i}, \hat{F}_{X_{i'}}), \text{BGSS} = \frac{1}{n} \sum_{1 \leq i < i' \leq n} d_W^2(\hat{F}_{X_i}, \hat{F}_{X_{i'}}) - \text{WGSS}.$$

We implement the  $k$ -W-means clustering using the R package `NbClust` (Charrad et al. 2014).

In what follows, we order clusters identified by  $k$ -W-means clustering according to the average transport ranks within each cluster in a descending order. Specifically, the first cluster having the largest average transport rank is the most central, while the last cluster having the smallest average transport rank corresponds to the most outlying cluster.

### 5.1 Simulations for Multivariate Gaussians

For  $p = 2$  and  $50$ , we sample  $n = 500$  observations  $\{X_i\}_{i=1}^n$  independently from a  $p$ -dimensional Gaussian distribution  $N(\boldsymbol{\mu}, \boldsymbol{\Sigma})$ , where  $\boldsymbol{\mu} = \mathbf{0}$  and  $\boldsymbol{\Sigma} = \text{diag}(p, p-1, \dots, 1)$ . The depth profiles  $\hat{F}_{X_i}$  (12) and transport ranks  $\hat{R}_{X_i}$  (13) are computed for each observation with  $d$  being the Euclidean metric in  $\mathbb{R}^p$ . For  $p = 2$ , the transport ranks (13) based on depth profiles capture the center-outward ordering of the 2-dimensional Gaussian data and are indeed highly correlated with the squared Mahalanobis distance from each observation  $X_i$  to the mean  $\boldsymbol{\mu}$ , i.e.  $(X_i - \boldsymbol{\mu})^\top \boldsymbol{\Sigma}^{-1} (X_i - \boldsymbol{\mu})$  (Figure 2). The  $k$ -W-means clustering based on the depth profiles partitions the data into  $k = 7$  clusters, lying from the closest to the farthest from the center  $\boldsymbol{\mu}$  (Figure 2); specifically, the Wasserstein barycenters of the depth profiles within each cluster (18) shift to the right from cluster 1 to cluster 7, indicating increased distances from the other observations. Figure 3 demonstrates similar findings for a simulated sample of  $n = 500$  observations from a 50-dimensional Gaussian distribution  $N(\boldsymbol{\mu}, \boldsymbol{\Sigma})$  with  $\boldsymbol{\mu} = \mathbf{0}$  and  $\boldsymbol{\Sigma} = \text{diag}(50, 49, \dots, 1)$ .

### 5.2 Simulations for Distributional Data

We consider a sample of  $n = 500$  one-dimensional Gaussian distributions  $\{N(\mu_i, \sigma_i^2)\}_{i=1}^n$  that are generated from a mixture of two distributions of distributions, i.e. there exist two groups of distributions. Specifically, we first generate  $Z_i \sim \text{Bernoulli}(p)$  and then sample  $\mu_i \sim N(-2, 0.5^2)$

### Object Depth Profiles & Transport Ranks

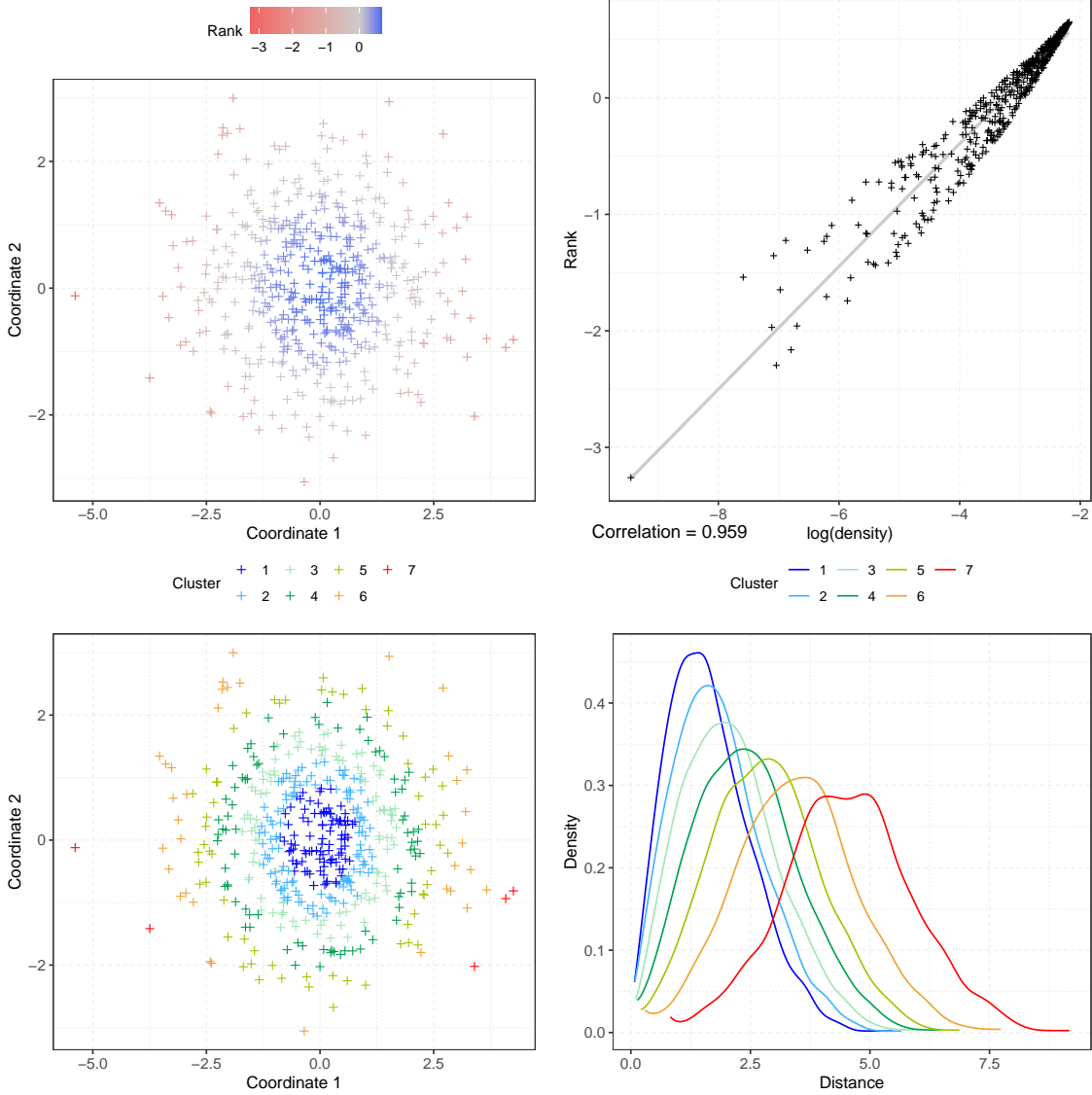


Figure 2: Scatter plots of a sample of  $n = 500$  observations generated from a 2-dimensional Gaussian distribution  $N(\mu, \Sigma)$  with  $\mu = \mathbf{0}$  and  $\Sigma = \text{diag}(2, 1)$ , where the points are colored according to their transport ranks (13) (top left) and  $k$ -W-means clustering (17) of the depth profiles  $\hat{F}_{X_i}$  (12) with  $\omega = X_i$  and  $d$  being the Euclidean metric (bottom left). Top right: Transport ranks versus logarithms of the density function of  $N(\mu, \Sigma)$  evaluated at each observation; the Pearson correlation is 0.959. Bottom right: Wasserstein barycenters of the depth profiles within each cluster (18).

if  $Z_i = 1$  and  $\mu_i \sim N(2, 0.5^2)$  if  $Z_i = 0$ ;  $\sigma_i \sim \text{Gamma}(2, 4)$ . Here,  $\text{Gamma}(\alpha, \beta)$  denotes a gamma distribution with shape  $\alpha$  and rate  $\beta$ . In addition, we consider balanced and unbalanced designs with  $p = 0.5$  and  $0.2$ , respectively.

When the design is balanced, distributions sampled from the two groups have similar depth

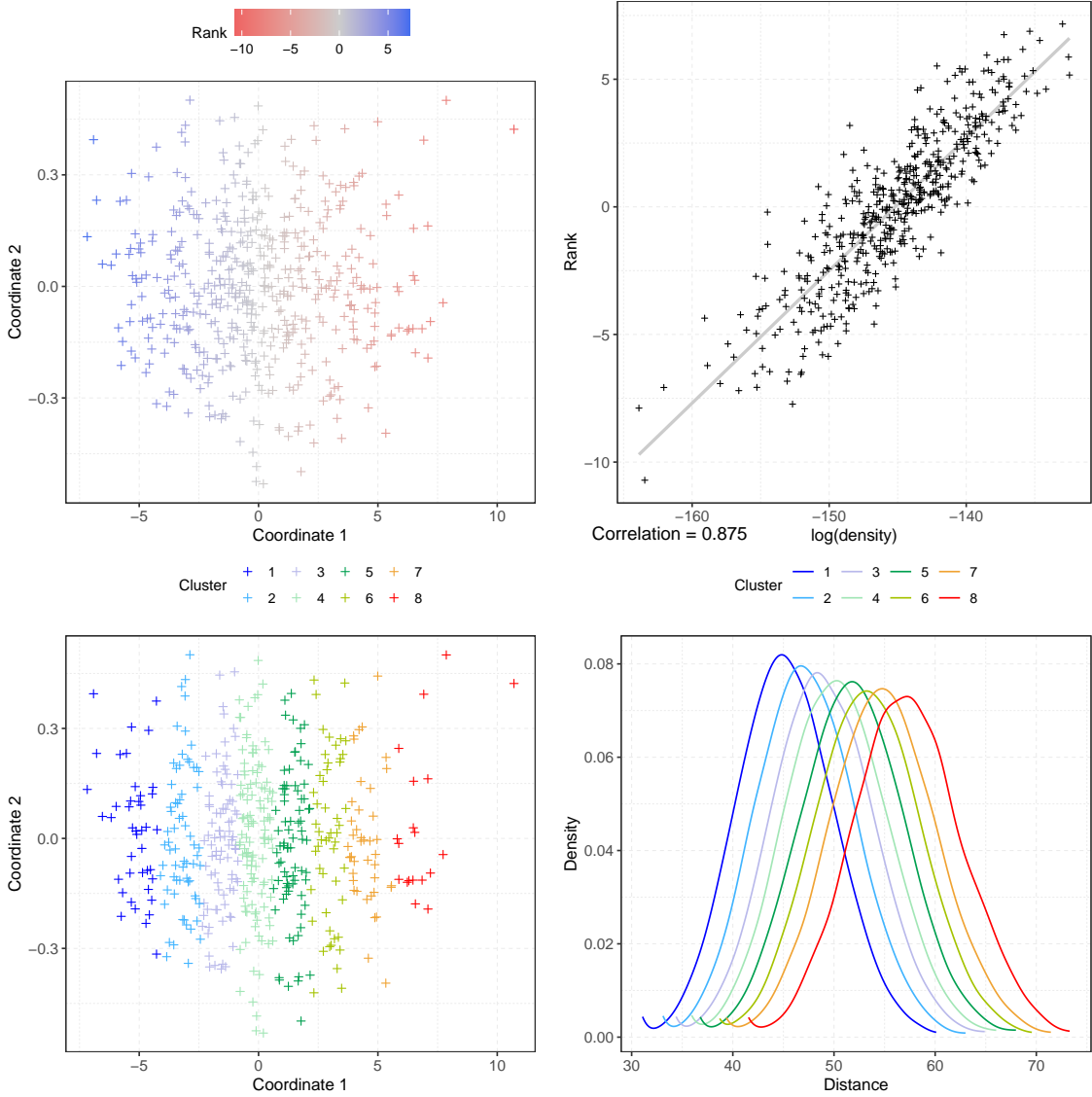


Figure 3: Two-dimensional MDS with respect to the Wasserstein metric  $d_W$  in (16) of the depth profiles  $\widehat{F}_{X_i}$  (12) with  $\omega = X_i$  of a sample of  $n = 500$  observations generated from a 50-dimensional Gaussian distribution  $N(\mu, \Sigma)$  with  $\mu = \mathbf{0}$  and  $\Sigma = \text{diag}(50, 49, \dots, 1)$ , where the points are colored according to their transport ranks (13) (top left) and  $k$ -W-means clustering (17) of the depth profiles  $\widehat{F}_{X_i}$  (bottom left). Top right: Transport ranks versus logarithms of the density function of  $N(\mu, \Sigma)$  evaluated at each observation, with Pearson correlation 0.874. Bottom right: Wasserstein barycenters of the depth profiles within each cluster (18).

profiles, and distributions lying closer to the empirical barycenter of all the 500 distributions have larger transport ranks. Hence it turns out as expected that the  $k$ -W-means clustering of the depth profiles cannot identify distributions sampled from the two different groups in this case. In contrast,

when  $p = 0.2$  and the design is unbalanced, the deepest observations in the sample lie in the larger subsample and the distributions in the smaller subsample have smaller transport ranks as compared to the other group. In addition, the  $k$ -W-means clustering almost perfectly distinguishes the two groups in the unbalanced case (Figure 4).

## 6 Data Applications

### 6.1 Human Mortality Data

Understanding human longevity has been of long-standing interest. A quantification is given by age-at-death distributions. We consider age-at-death distributions for different countries, which are obtained from the Human Mortality Database (<http://www.mortality.org>) for the year 2000 for  $n = 34$  countries (or areas), separately for males and females. For this sample of distributional data we adopt the Wasserstein metric  $d_W$  (16). To analyze the data geometry of this sample of distributions  $\{X_i\}_{i=1}^{34}$  we obtained depth profiles  $\widehat{F}_{X_i}$  (12) with  $\omega = X_i$  for each country. Applying  $k$ -W-means clustering to the depth profiles for age-at-death distributions of females and males, the results are shown together with the transport ranks in Figures 5 and 6, respectively.

We visualize the results with *nested circle plots*, where points representing observations  $\{X_i\}_{i=1}^n$  are placed on nested circles such that each cluster takes up one circle. In addition, the locations of each observation on a circle are determined by two-dimensional classical/metric multidimensional scaling (MDS) (Mardia 1978) of observations, i.e., MDS with respect to the Wasserstein metric  $d_W$  (16) of the age-at-death distributions in this case. We will refer to this application of MDS as *object MDS*. Specifically, we implement MDS using the function `cmdscale()` in the R build-in package `stats` (R Core Team 2020). In terms of polar coordinates, angles of points on a nested circle plot are equal to the angles of the corresponding observations on the MDS plot, and radii are determined by the clusters to which the observations belong. Hence, nested circle plots reflect both the similarity of individual observations in terms of the distance of the metric space where the observations take values and also the center-outward ordering as provided by their transport ranks. We note that in the top two panels of Figures 5–6 MDS is applied to the estimated depth

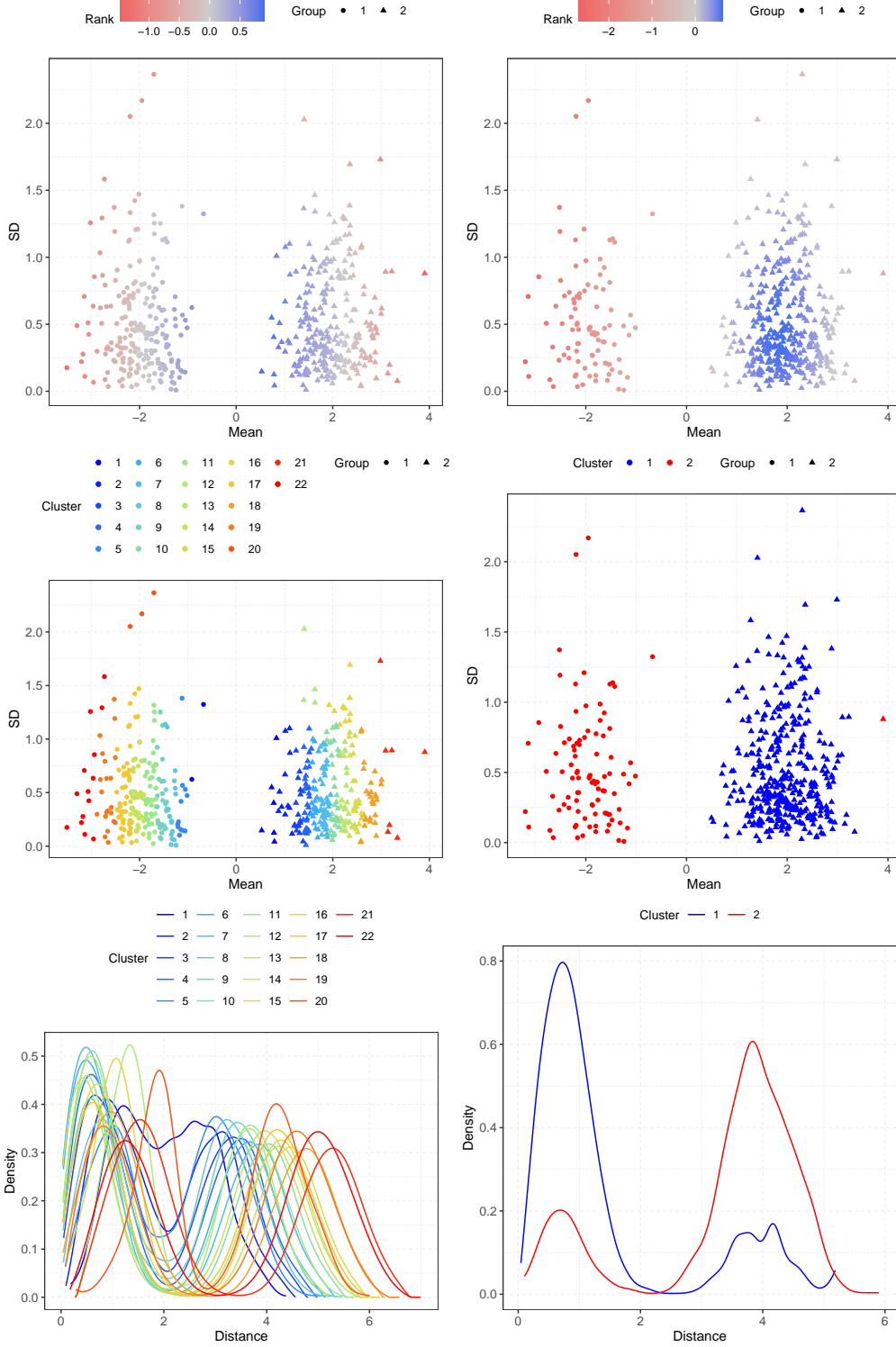


Figure 4: Analysis of samples of  $n = 500$  one-dimensional Gaussian distributions  $\{N(\mu_i, \sigma_i^2)\}_{i=1}^n$  with  $p = 0.5$  (left) and  $0.2$  (right), respectively. Top two rows: Scatterplots of mean  $\mu_i$  and standard deviation ( $\sigma_i$ ), where the points are colored according to the transport ranks (13) (top) and the  $k$ -W-means clustering (17) of the depth profiles  $\widehat{F}_{X_i}$  (12) with  $\omega = X_i$  (middle). Bottom: Wasserstein barycenters of the depth profiles  $\widehat{F}_{X_i}$  for the distributions within each cluster.

### Object Depth Profiles & Transport Ranks

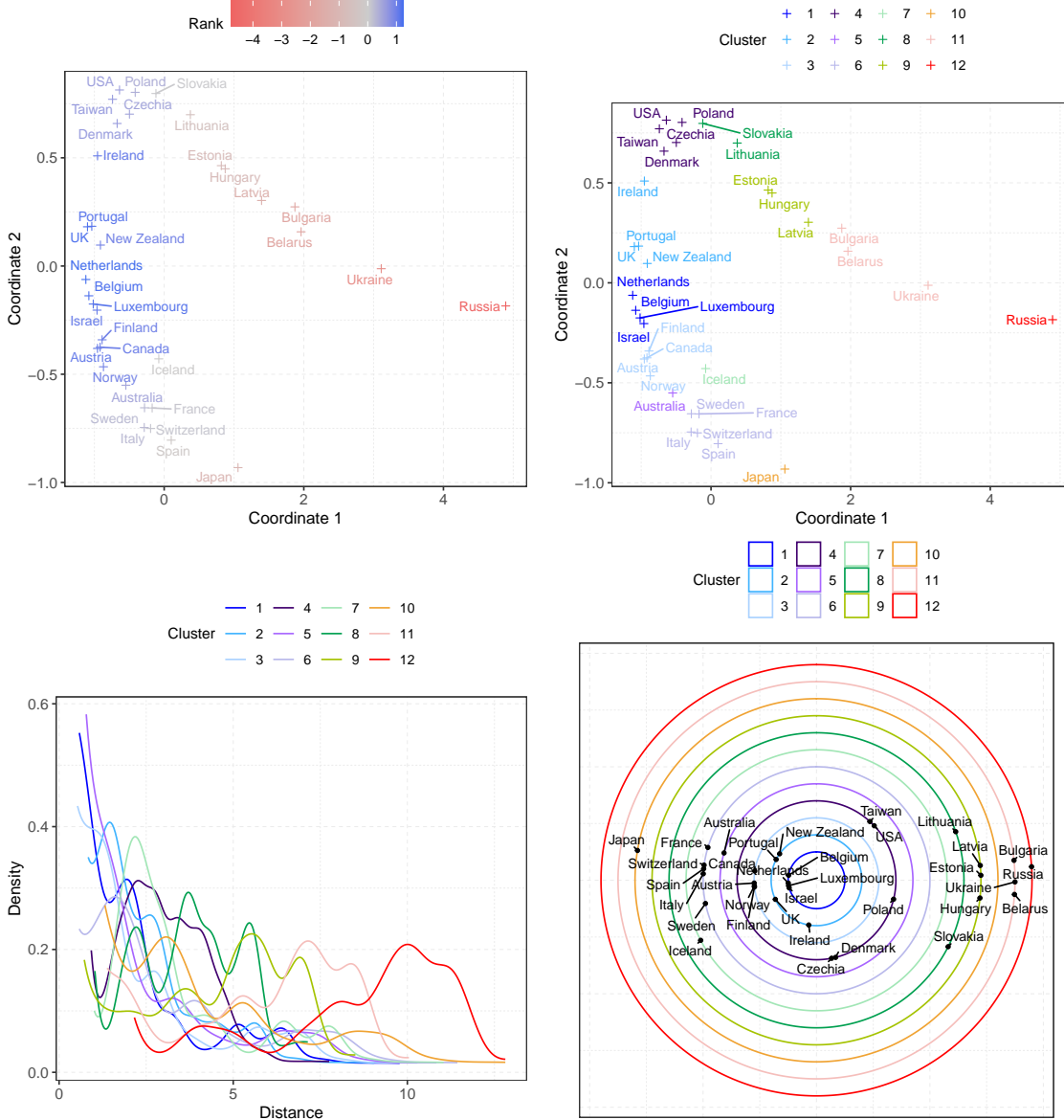


Figure 5: Top: Two-dimensional MDS with respect to the Wasserstein metric  $d_W$  in (16) of the depth profiles  $\hat{F}_{X_i}$  (12) with  $\omega = X_i$  of the age-at-death distributions of females in 2000 for the 34 countries, where the points are colored according to the  $k$ -W-means clustering (17) of the depth profiles  $\hat{F}_{X_i}$  (12) with  $\omega = X_i$  (left) and their transport ranks (13) (right). Bottom left: Wasserstein barycenters of the depth profiles  $\hat{F}_{X_i}$  for the age-at-death distributions of females in 2000 within each cluster. Bottom right: Nested circle plot for the age-at-death distributions of females in 2000.

profiles  $\hat{F}_{X_i}$  with metric  $d_W$ , referred to as *depth MDS*, in contrast to object MDS, which is applied to the observations  $X_i$  themselves, with metric  $d$  in  $\Omega$ ; in this particular example  $d = d_W$ .

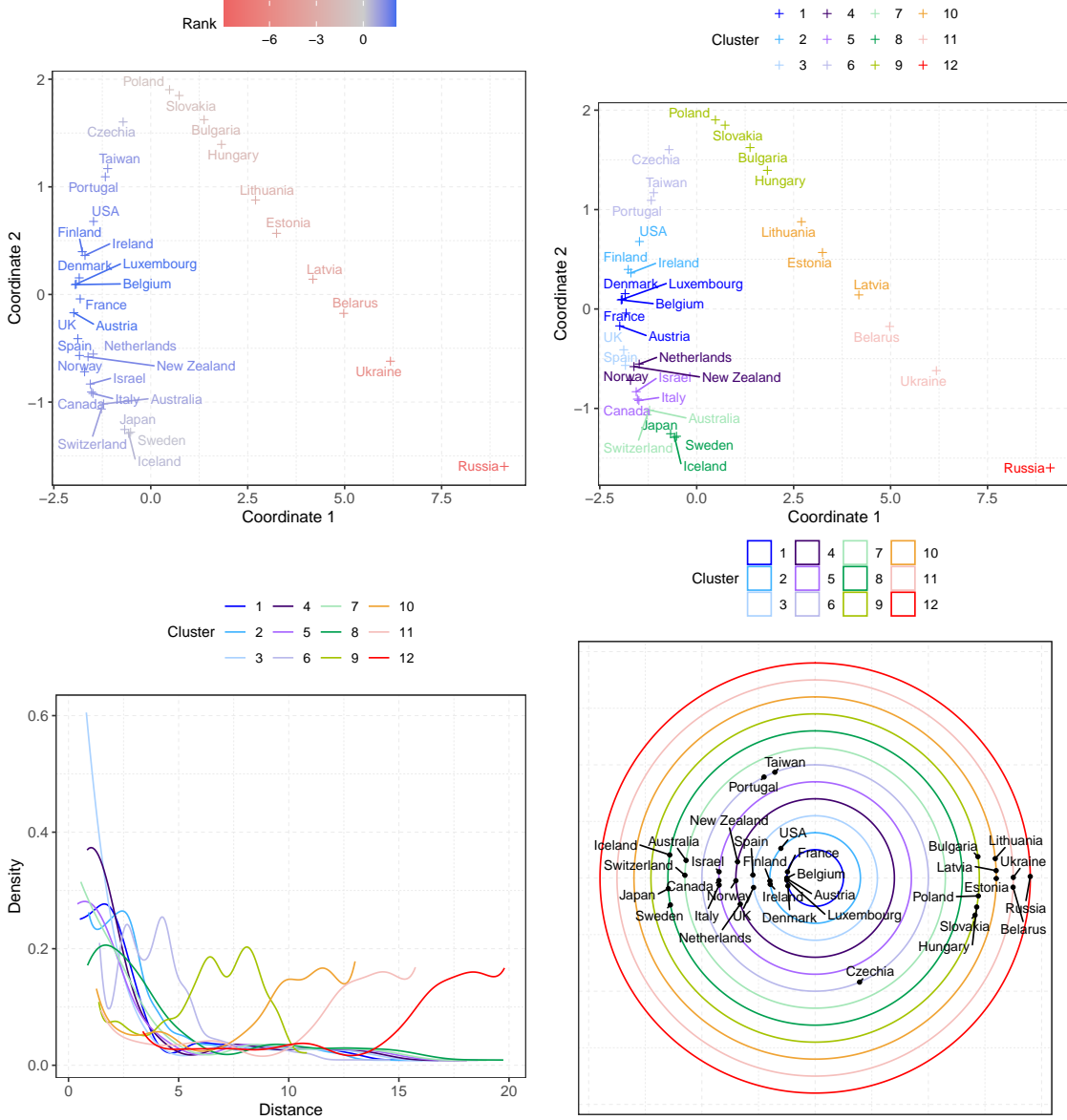


Figure 6: Top: Two-dimensional MDS with respect to the Wasserstein metric  $d_W$  in (16) of the depth profiles  $\widehat{F}_{X_i}$  (12) with  $\omega = X_i$  of the age-at-death distributions of males in 2000 for the 34 countries, where the points are colored according to the  $k$ -W-means clustering (17) of the depth profiles  $\widehat{F}_{X_i}$  (12) with  $\omega = X_i$  (left) and their transport ranks (13) (right). Bottom left: Wasserstein barycenters of the depth profiles  $\widehat{F}_{X_i}$  for the age-at-death distributions of males in 2000 within each cluster. Bottom right: Nested circle plot for the age-at-death distributions of males in 2000.

For both females and males, two groups of countries stand out in terms of depth profiles as compared to the others: One group includes Japan, Switzerland and Sweden; and the other one Eastern European countries, such as Russia, Ukraine, Belarus, Latvia and Estonia. While these

two groups are both outlying, the former group is characterized by enhanced longevity and the latter by reduced longevity. Luxembourg and Belgium belong to the most central cluster for both females and males. Iceland and Spain are among the most outlying countries for one gender only, with highest longevity for males in Iceland and for females in Spain. France and Israel belong to the most central cluster for males and females, respectively, but are more outlying for females and males, respectively. Overall, as shown in the bottom left panels of Figures 5–6, the age-at-death distributions for males for the outlying countries are much farther away from the others than those of females. In particular, the empirical Fréchet variance of the depth profiles,  $n^{-1} \sum_{i=1}^n d_W^2(\widehat{F}_{X_i}, \widehat{F}_\oplus)$ , of age-at-death distributions for females and males of different countries is 2.08 and 8.22, respectively, where  $\widehat{F}_\oplus = \operatorname{argmin}_{\omega \in \mathcal{W}} \sum_{i=1}^n d_W^2(\widehat{F}_{X_i}, \omega)$  is the empirical Fréchet mean of the depth profiles.

## 6.2 U.S. Electricity Generation Data

Compositional data comprise another type of data that do not lie in a vector space. Such data are commonly encountered and consist of vectors of nonnegative elements that sum up to 1. Examples include geochemical compositions and microbiome data. Various approaches to handle the nonlinearity that is inherent in such data have been developed (Aitchison 1986; Scealy and Welsh 2014). We consider here the U.S. electricity generation data which are publicly available on the website of the U.S. Energy Information Administration (<http://www.eia.gov/electricity>). The data consist of net generation of electricity from different sources for each state. Here, we consider the data for the year 2000. In preprocessing, we excluded the “pumped storage” category due to errors in these data and then merged the energy sources into three categories: Natural Gas, consisting of “natural gas” alone; Other Fossil, consisting of “coal”, “petroleum” and “other gases”; Renewables and Nuclear, combining the remaining sources “hydroelectric conventional”, “solar thermal and photovoltaic”, “geothermal”, “wind”, “wood and wood derived fuels”, “other biomass”, “nuclear” and “other”. Hence, we have a sample of  $n = 50$  observations  $\{X_i\}_{i=1}^n$ , each of which takes values in a 2-simplex  $\Delta^2 = \{\mathbf{x} \in \mathbb{R}^3 : \mathbf{x}^\top \mathbf{1}_3 = 1\}$ , where  $\mathbf{1}_3 = (1, 1, 1)^\top$ . Since the component-wise square root  $\sqrt{\mathbf{x}} = (\sqrt{x_1}, \sqrt{x_2}, \sqrt{x_3})^\top$  of an element  $\mathbf{x} \in \Delta^2$  lies in the sphere  $\mathcal{S}^2$ , we adopt the geodesic

metric on this sphere

$$d_S(\mathbf{x}, \mathbf{y}) = \arccos(\sqrt{\mathbf{x}}^\top \sqrt{\mathbf{y}}), \text{ for } \mathbf{x}, \mathbf{y} \in \Delta^2. \quad (19)$$

We then compared the estimated transport ranks (13) for each state with the angular Tukey depths (ATDs, Liu and Singh 1992) of  $\{\sqrt{X_i}\}_{i=1}^n$ . Overall, the proposed transport ranks and ATDs yield similar center-outward ordering of the 50 states for these data (Figure 7). Maryland emerges as the transport median and is also at the median for ATDs. On closer inspection one finds some interesting discrepancies between transport ranks and the ATD measure of outlyingness, especially for the states that are relatively close or far away from the center Maryland in terms of their outlyingness. The states near Maryland, as shown in orange and light violet in the bottom panels of Figure 7, all have high transport ranks, while their ATDs vary widely. In particular, Montana, with an electricity generation pattern very similar to that of Maryland, has the lowest ATD level while it has a high transport rank. A subset of states that are colored in turquoise and light violet in the bottom panels of Figure 7 have the lowest ATDs among all states but have a much wider range of transport ranks. For example, Hawaii and Delaware which are not far from Maryland in terms of energy generation, have high transport ranks and low ATD levels. The overall conclusion is that transport ranks are much better suited than ATDs for studying the geometry of this data set and for quantifying outlyingness.

Figure 8 shows the  $k$ -W-means clustering results for the depth profiles of the electricity generation compositions; the 50 states are divided into three clusters. Most states mainly use the Other Fossil source in electricity generation rather than Natural Gas; the latter is considered to be the cleanest fossil fuel source (Faramawy et al. 2016). The states with highest centrality in terms of the proposed transport ranks utilize little Natural Gas and similar amounts of Other Fossil and Renewables and Nuclear. In contrast, California, Idaho, Rhode Island, and Vermont are grouped into the most outlying transport rank cluster, as they utilize the smallest fraction of the (undesirable) Other Fossil source.

### Object Depth Profiles & Transport Ranks

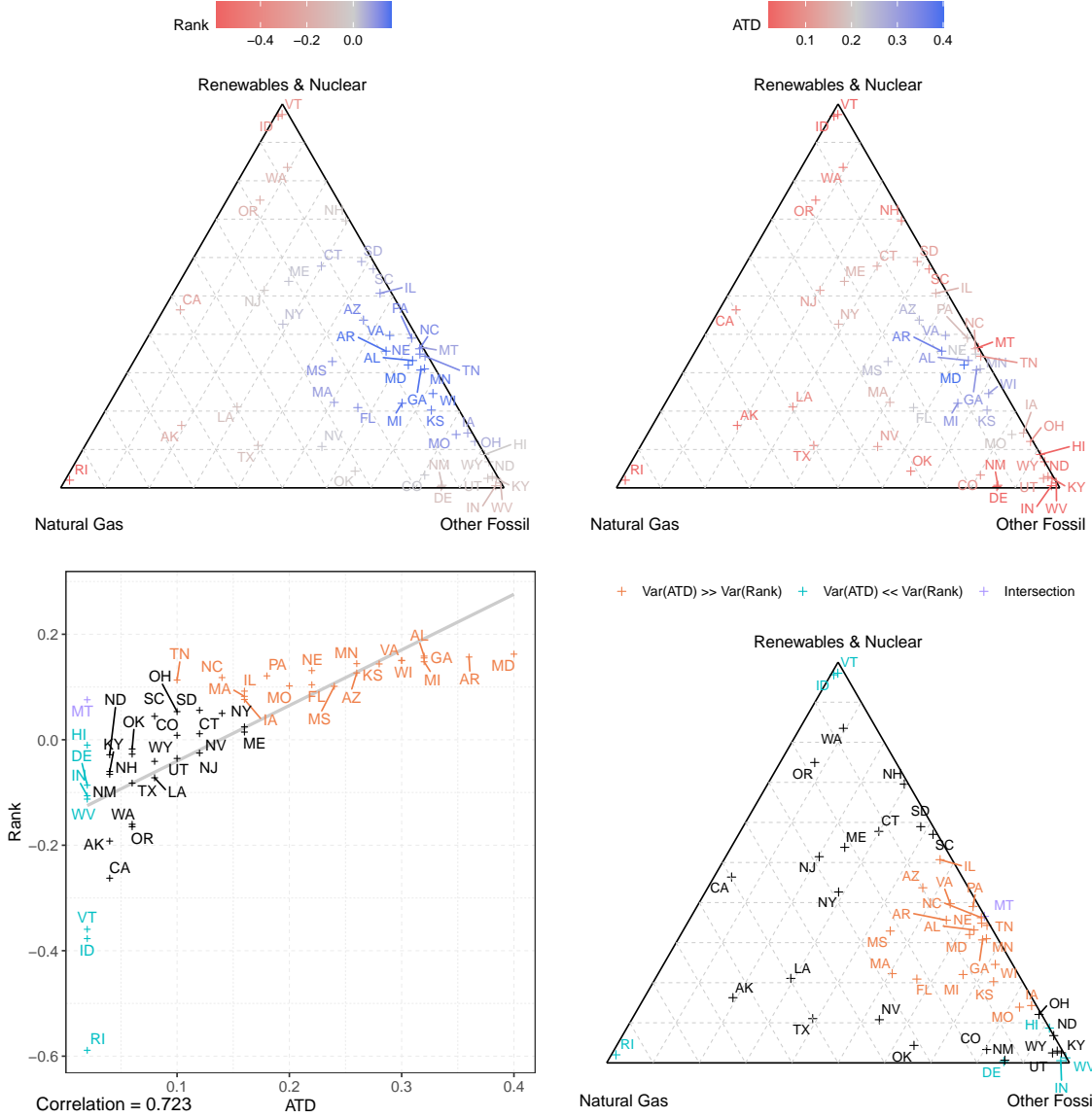


Figure 7: Ternary plot of compositions of electricity generation in the year 2000 for the 50 states in the U.S.. Color indicates transport ranks (13) (top left) and ATD levels (top right). The Pearson correlation between the transport ranks and the values of the log density function is 0.723 and the straight line in the bottom left panel shows the least squares fit (just to provide a perspective). In the bottom two panels, a subset of states with similarly small ATDs but different transport ranks is highlighted in orange, and another subset with similarly high transport ranks but different ATDs is highlighted in turquoise; the intersection of the two subsets is colored in light violet.

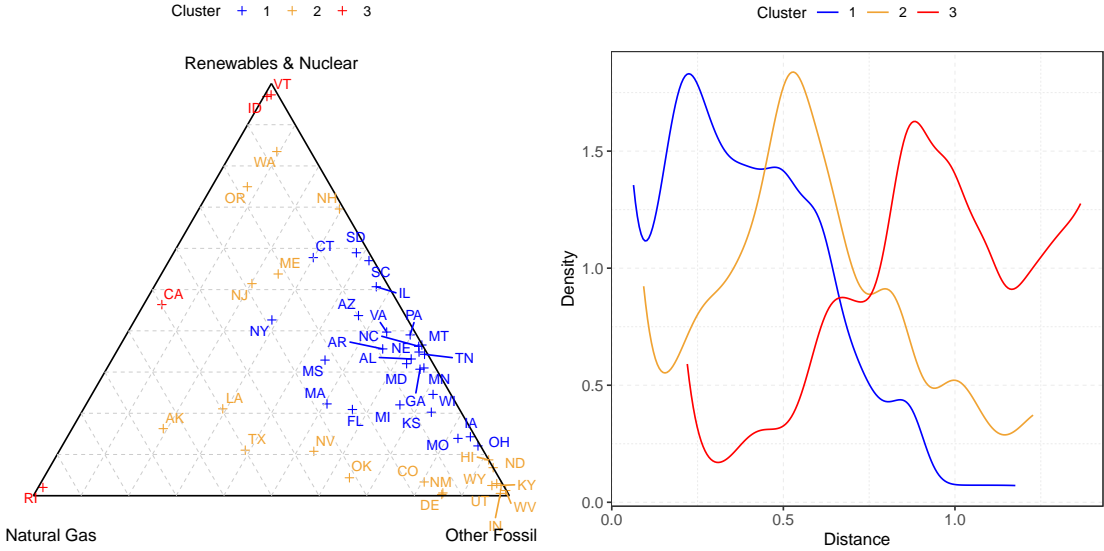


Figure 8: Left: Ternary plot of compositions of electricity generation in 2000 for the 50 U.S. states in the U.S.; points are colored according to  $k$ -W-means clustering (17) of the depth profiles  $\widehat{F}_{X_i}$  (12) with  $\omega = X_i$  and  $d = d_S$  in (19). Right: Wasserstein barycenters of the depth profiles within each cluster (18).

### 6.3 Manhattan Yellow Taxi Data

Yellow taxi trip records in New York City (NYC) including pick-up and drop-off dates/times, pick-up and drop-off locations, and driver-reported passenger counts are available at <http://www1.nyc.gov/site/tlc/about/tlc-trip-record-data.page>). We focus on the data pertaining to Manhattan and, excluding Governor's Island, Ellis Island, and Liberty Island, divide the remaining 66 zones of Manhattan into 13 regions (Table ?? in the Supplement). Of interest are networks that represent how many people traveled between these areas during a day. To this end, we construct networks for yellow taxi trips between the 13 regions for each day in the year 2019, obtaining a 13-dimensional graph adjacency matrix for each day, where each entry holds the edge weight given by the total number of passengers traveling between the two corresponding regions within the given day. The edge weights are then normalized by the maximum edge weight for each day so that they lie in  $[0, 1]$ . We choose the Frobenius metric  $d_F$  as metric between the graph adjacency matrices,

$$d_F(\mathbf{R}_1, \mathbf{R}_2) = \left\{ \text{trace} \left[ (\mathbf{R}_1 - \mathbf{R}_2)(\mathbf{R}_1 - \mathbf{R}_2)^\top \right] \right\}^{1/2}, \text{ for } \mathbf{R}_1, \mathbf{R}_2 \in \mathbb{R}^{13 \times 13}. \quad (20)$$

Weekdays are found to have lower transport ranks and are more central, while weekends have higher transport ranks and are more outlying (Figure 9). The  $k$ -W-means clustering of the depth profiles yields two clusters, which almost entirely correspond to weekdays and weekends, respectively. Only twelve days are included in “opposite” clusters. Among these, Independence Day, July 5, Veterans Day, and New Year’s Eve are weekdays but also holidays or a Friday after a holiday. Every weekday between September 23 and September 30, including September 23–26, was designated as a “gridlock alert day” by the NYC Department of Transportation, due to the UN General Assembly meetings held from September 24 through 30, i.e. these are the days likely to feature the heaviest traffic of the year. May 12 was Japan Day, which is an annual event hosted by Japanese community of New York including a wide range of activities throughout the day; likely December 21 and 22 had traffic congestion due to the impending holidays. So it is not surprising that these three days were assigned to the weekday cluster.

## 7 Discussion

In this paper we introduce a new toolbox for the analysis of metric space valued data or random objects. Key tools are the depth profiles, transport ranks and transport median sets. Depth profiles are canonical and straightforward and their combination with optimal transport leads to transport ranks in a natural way. Transport ranks can then be harnessed to arrive at a notion of data depth. Depth profiles along with  $k$ -W-means clustering also lend themselves for the construction of level sets that correspond to these clusters and ultimately a notion of quantiles for random object data. Apart from opening a new arena for future explorations of general metric-space valued data, the proposed toolbox may also be of interest for revisiting data analysis in classical Euclidean spaces; for example it leads to a notion of depth that has not been hitherto explored in these more traditional spaces. While the notions we introduce are population based, sample based estimators can be easily and efficiently constructed. Theoretical analysis shows that they converge to their population targets.

This new approach is supported by theory for a wide class of metric spaces in conjunction with

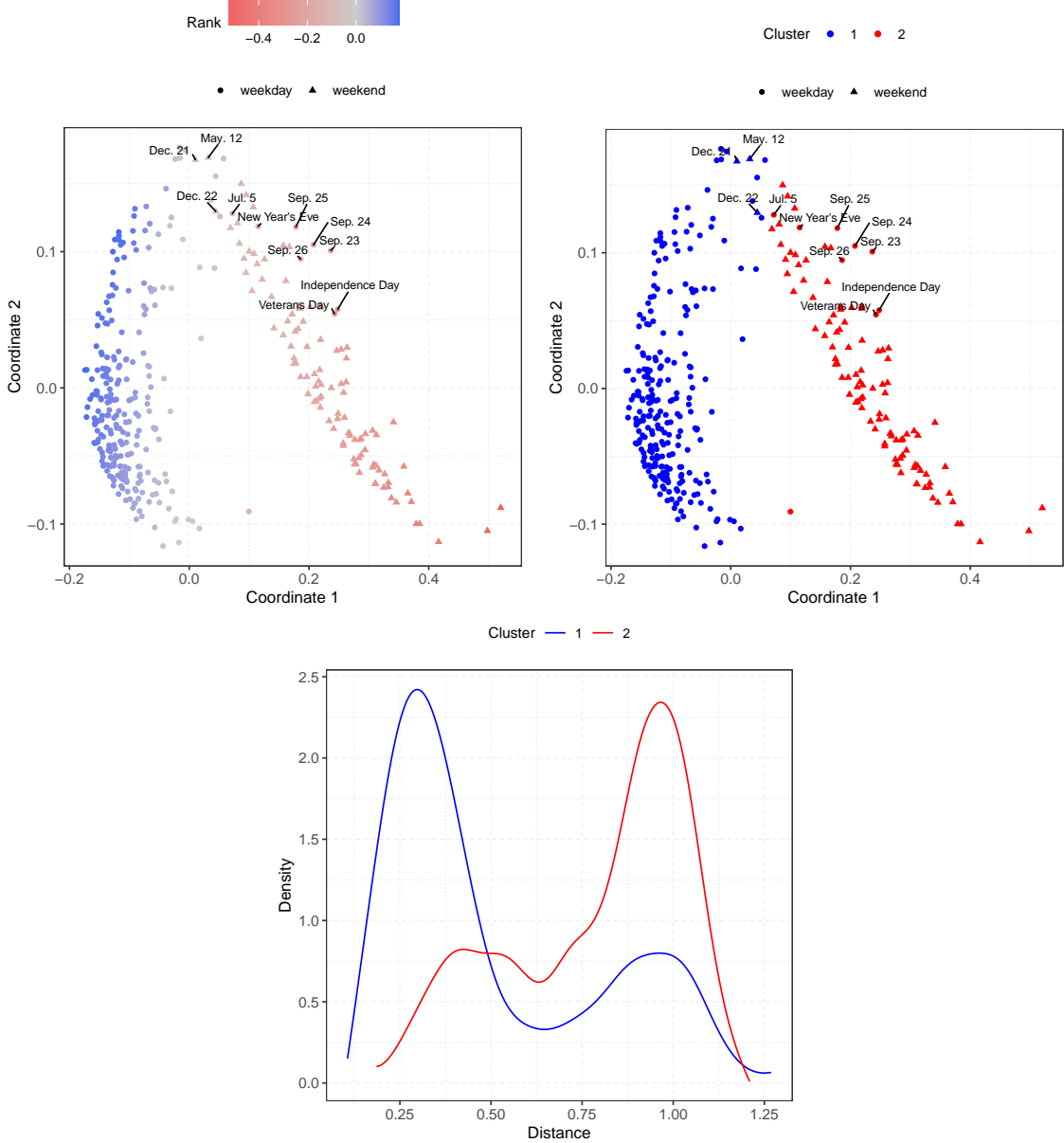


Figure 9: Two-dimensional MDS of the depth profiles of the daily Manhattan Yellow Taxi transport networks in 2019 with normalized edge weights, where the points are colored according to their transport ranks (13) (top left) and  $k$ -W-means clustering (17) of the depth profiles  $\widehat{F}_{X_i}$  (12) with  $\omega = X_i$  and  $d = d_F$  in (20) (top right). Bottom: Wasserstein barycenters of the depth profiles within each cluster.

a probability measure defined on the space, as long as an entropy condition is satisfied and the spaces are totally bounded and separable. While this does place a restriction on the spaces where the proposed tools are supported by theory, we show that many complex spaces of practical interest

such as distributional data, networks and tree spaces are covered under mild regularity conditions. From a practical perspective, as long as one can compute pairwise distances, the proposed tools can be applied for all kinds of exploratory data analysis tasks for metric space valued data, for example the identification of data medians or outliers. The data examples clearly demonstrate the utility of the proposed tools for distributional, compositional and network data.

Various extensions will be of interest for future research. For example, to understand the interplay between depth profiles and distances between objects in  $\Omega$  one may work with generalizations of the transport rank  $R_\omega$ , the *generalized transport rank*  $R_\omega^\psi$ , as

$$R_\omega^\psi = \mathbb{E} \left\{ \psi(d(\omega, X)) \text{sign} \left( \int_0^1 [F_X^{-1}(u) - F_\omega^{-1}(u)] du \right) \int_0^1 |F_X^{-1}(u) - F_\omega^{-1}(u)| du \right\},$$

where  $\psi(\cdot)$  is a weight function which can be tuned depending on the goal of the data analysis. Through  $\psi(d(\omega, X))$  one may emphasize either observations closer to  $\omega$  or those farther from  $\omega$ . One may also consider other distributional metrics  $m(F_X, F_\omega)$  to gauge the distance between depth profiles and to derive transport ranks, level sets and quantiles. Other extensions of interest concern modes and medians of random objects, extending implementations and theory for transport median sets.

## References

Aitchison, J. (1986). *The Statistical Analysis of Compositional Data*. Chapman & Hall, Ltd.

Ambrosio, L., N. Gigli, and G. Savaré (2008). *Gradient Flows in Metric Spaces and in the Space of Probability Measures*. Springer.

Barnett, V. (1976). The ordering of multivariate data. *Journal of the Royal Statistical Society: Series A (General)* 139(3), 318–344.

Billera, L. J., S. P. Holmes, and K. Vogtmann (2001). Geometry of the space of phylogenetic trees. *Advances in Applied Mathematics* 27(4), 733–767.

Blei, R., F. Gao, and W. Li (2007). Metric entropy of high dimensional distributions. *Proceedings of the American Mathematical Society* 135(12), 4009–4018.

Caliński, T. and J. Harabasz (1974). A dendrite method for cluster analysis. *Communications in Statistics 3*(1), 1–27.

Charrad, M., N. Ghazzali, V. Boiteau, and A. Niknafs (2014). NbClust: An R package for determining the relevant number of clusters in a data set. *Journal of Statistical Software 61*(6), 1–36.

Chau, J., H. Ombao, and R. von Sachs (2019). Intrinsic data depth for Hermitian positive definite matrices. *Journal of Computational and Graphical Statistics 28*(2), 427–439.

Chen, J., K. Bittinger, E. S. Charlson, C. Hoffmann, J. Lewis, G. D. Wu, R. G. Collman, F. D. Bushman, and H. Li (2012). Associating microbiome composition with environmental covariates using generalized UniFrac distances. *Bioinformatics 28*(16), 2106–2113.

Chen, M., C. Gao, and Z. Ren (2018). Robust covariance and scatter matrix estimation under Huber’s contamination model. *The Annals of Statistics 46*(5), 1932–1960.

Cholaquidis, A., R. Fraiman, F. Gamboa, and L. Moreno (2020). Weighted lens depth: Some applications to supervised classification. *arXiv preprint arXiv:2011.11140*.

Claeskens, G., M. Hubert, L. Slaets, and K. Vakili (2014). Multivariate functional halfspace depth. *Journal of the American Statistical Association 109*(505), 411–423.

Dai, X. and S. Lopez-Pintado (2021). Tukey’s depth for object data. *arXiv preprint arXiv:2109.00493*.

Dryden, I. L., A. Koloydenko, and D. Zhou (2009). Non-Euclidean statistics for covariance matrices, with applications to diffusion tensor imaging. *The Annals of Applied Statistics 3*, 1102–1123.

Dutta, S., A. K. Ghosh, and P. Chaudhuri (2011). Some intriguing properties of Tukey’s half-space depth. *Bernoulli 17*(4), 1420–1434.

Dyckerhoff, R. (2004). Data depths satisfying the projection property. *Allgemeines Statistisches Archiv 88*(2), 163–190.

Faramawy, S., T. Zaki, and A.-E. Sakr (2016). Natural gas origin, composition, and processing: A review. *Journal of Natural Gas Science and Engineering 34*, 34–54.

Fraiman, R. and G. Muniz (2001). Trimmed means for functional data. *Test 10*(2), 419–440.

Fréchet, M. (1948). Les éléments aléatoires de nature quelconque dans un espace distancié. *Annales*

de l’Institut Henri Poincaré 10, 215–310.

Gao, F. and J. A. Wellner (2009). On the rate of convergence of the maximum likelihood estimator of a k-monotone density. *Science in China Series A: Mathematics* 52(7), 1525–1538.

Geenens, G., A. Nieto-Reyes, and G. Francisci (2021). Statistical depth in abstract metric spaces. *arXiv preprint arXiv:2107.13779*.

Ghosh, A. K. and P. Chaudhuri (2005). On maximum depth and related classifiers. *Scandinavian Journal of Statistics* 32(2), 327–350.

Gijbels, I. and S. Nagy (2017). On a general definition of depth for functional data. *Statistical Science* 32(4), 630–639.

Ginestet, C. E., J. Li, P. Balachandran, S. Rosenberg, and E. D. Kolaczyk (2017). Hypothesis testing for network data in functional neuroimaging. *The Annals of Applied Statistics*, 725–750.

Jeon, J. M. and B. U. Park (2020). Additive regression with Hilbertian responses. *The Annals of Statistics* 48(5), 2671–2697.

Jiang, X., L.-H. Lim, Y. Yao, and Y. Ye (2011). Statistical ranking and combinatorial Hodge theory. *Mathematical Programming* 127(1), 203–244.

Jörnsten, R. (2004). Clustering and classification based on the  $L_1$  data depth. *Journal of Multivariate Analysis* 90(1), 67–89.

Kim, J., N. A. Rosenberg, and J. A. Palacios (2020). Distance metrics for ranked evolutionary trees. *Proceedings of the National Academy of Sciences* 117(46), 28876–28886.

Kleindessner, M. and U. von Luxburg (2017). Lens depth function and  $k$ -relative neighborhood graph: Versatile tools for ordinal data analysis. *Journal of Machine Learning Research* 18(58), 1–52.

Kolaczyk, E. D., L. Lin, S. Rosenberg, J. Walters, and J. Xu (2020). Averages of unlabeled networks: Geometric characterization and asymptotic behavior. *The Annals of Statistics* 48(1), 514–538.

Koshevoy, G. and K. Mosler (1997). Zonoid trimming for multivariate distributions. *The Annals of Statistics* 25(5), 1998–2017.

Lange, T., K. Mosler, and P. Mozharovskyi (2014). Fast nonparametric classification based on data depth. *Statistical Papers* 55(1), 49–69.

Li, J., J. A. Cuesta-Albertos, and R. Y. Liu (2012). DD-classifier: Nonparametric classification procedure based on DD-plot. *Journal of the American Statistical Association* 107(498), 737–753.

Li, J. and R. Y. Liu (2004). New nonparametric tests of multivariate locations and scales using data depth. *Statistical Science* 19(4), 686–696.

Lin, Z. and H.-G. Müller (2021). Total variation regularized Fréchet regression for metric-space valued data. *The Annals of Statistics, in press*.

Liu, R. Y. (1990). On a notion of data depth based on random simplices. *The Annals of Statistics* 18(1), 405–414.

Liu, R. Y., J. M. Parelius, and K. Singh (1999). Multivariate analysis by data depth: Descriptive statistics, graphics and inference (with discussion and a rejoinder by Liu and Singh). *The Annals of Statistics* 27(3), 783–858.

Liu, R. Y. and K. Singh (1992). Ordering directional data: Concepts of data depth on circles and spheres. *The Annals of Statistics* 20(3), 1468–1484.

Liu, Z. and R. Modarres (2011). Lens data depth and median. *Journal of Nonparametric Statistics* 23(4), 1063–1074.

Liu, Z., R. Modarres, and M. Yang (2013). A multivariate control quantile test using data depth. *Computational Statistics & Data Analysis* 57(1), 262–270.

López-Pintado, S. and J. Romo (2009). On the concept of depth for functional data. *Journal of the American Statistical Association* 104(486), 718–734.

López-Pintado, S. and J. Romo (2011). A half-region depth for functional data. *Computational Statistics & Data Analysis* 55(4), 1679–1695.

Lunagómez, S., S. C. Olhede, and P. J. Wolfe (2020). Modeling network populations via graph distances. *Journal of the American Statistical Association*, 1–18.

Mardia, K. V. (1978). Some properties of classical multi-dimensional scaling. *Communications in Statistics - Theory and Methods* 7(13), 1233–1241.

Mosler, K. (2013). Depth statistics. In C. Becker, R. Fried, and S. Kuhnt (Eds.), *Robustness and Complex Data Structures*, pp. 17–34. Springer.

Mosler, K. and P. Mozharovskyi (2021). Choosing among notions of multivariate depth statistics.

*Statistical Science*. in press.

Mosler, K. and Y. Polyakova (2012). General notions of depth for functional data. *arXiv preprint arXiv:1208.1981*.

Nagy, S., I. Gijbels, M. Omelka, and D. Hlubinka (2016). Integrated depth for functional data: Statistical properties and consistency. *ESAIM: Probability and Statistics* 20, 95–130.

Nieto-Reyes, A. and H. Battey (2016). A topologically valid definition of depth for functional data. *Statistical Science* 31(1), 61–79.

Oja, H. (1983). Descriptive statistics for multivariate distributions. *Statistics & Probability Letters* 1(6), 327–332.

Paindaveine, D. and G. Van Bever (2013). From depth to local depth: A focus on centrality. *Journal of the American Statistical Association* 108(503), 1105–1119.

Paindaveine, D. and G. Van Bever (2018). Halfspace depths for scatter, concentration and shape matrices. *The Annals of Statistics* 46(6B), 3276–3307.

Pan, W., X. Wang, H. Zhang, H. Zhu, and J. Zhu (2020). Ball covariance: A generic measure of dependence in Banach space. *Journal of the American Statistical Association* 115(529), 307–317.

Petersen, A., H.-G. Müller, et al. (2019). Fréchet regression for random objects with euclidean predictors. *The Annals of Statistics* 47(2), 691–719.

R Core Team (2020). *R: A Language and Environment for Statistical Computing*. Vienna, Austria: R Foundation for Statistical Computing.

Rousseeuw, P. J. and M. Hubert (1999). Regression depth. *Journal of the American Statistical Association* 94(446), 388–402.

Rousseeuw, P. J., I. Ruts, and J. W. Tukey (1999). The bagplot: A bivariate boxplot. *The American Statistician* 53(4), 382–387.

Sealby, J. and A. Welsh (2014). Colours and cocktails: Compositional data analysis. *Australian & New Zealand Journal of Statistics* 56(2), 145–169.

Serfling, R. (2002). A depth function and a scale curve based on spatial quantiles. In *Statistical Data Analysis Based on the L<sub>1</sub>-Norm and Related Methods*, pp. 25–38. Springer.

Thanwerdas, Y. and X. Pennec (2021).  $O(n)$ -invariant Riemannian metrics on SPD matrices. *arXiv*

*preprint arXiv:2109.05768.*

Tukey, J. W. (1975). Mathematics and the picturing of data. In *Proceedings of the International Congress of Mathematicians*, Volume 2, pp. 523–531. Canadian Mathematical Congress.

van der Vaart, A. and J. Wellner (1996). *Weak Convergence and Empirical Processes*. Springer, New York.

Wang, X., J. Zhu, W. Pan, J. Zhu, and H. Zhang (2021). Nonparametric statistical inference via metric distribution function in metric spaces. *arXiv preprint arXiv:2107.07317*.

Yang, M. and R. Modarres (2018).  $\beta$ -skeleton depth functions and medians. *Communications in Statistics—Theory and Methods* 47(20), 5127–5143.

Zhang, J. (2002). Some extensions of Tukey’s depth function. *Journal of Multivariate Analysis* 82(1), 134–165.

Zuo, Y. and R. Serfling (2000). General notions of statistical depth function. *The Annals of Statistics* 28(2), 461–482.